HOLOCENE

The Holocene

Holocene sea-ice conditions and circulation at the Chukchi-Alaskan margin, Arctic Ocean, inferred from biomarker proxies

Journal:	*The Holocene*
Manuscript ID	HOL-15-0080.R2
Manuscript Type:	Paper
Date Submitted by the Author:	n/a
Complete List of Authors:	Polyak, Leonid; Ohio State University, Byrd Polar and Climate Research Center Belt, Simon; University of Plymouth, Petroleum and Environmental Geochemistry Group Cabedo-Sanz, Patricia; University of Plymouth, Petroleum and Environmental Geochemistry Group Yamamoto, Masanobu; Hokkaido University, Faculty of Environmental Earth Science Park, Yu-Hyeon; Hokkaido University, Graduate School of Environmental Science
Keywords:	Chukchi Sea, western Arctic, Holocene, sea-ice history, biomarker proxies, IP25
Abstract:	Two sediment cores from the Chukchi Sea margin were investigated for the Arctic sea ice biomarker IP25, along with marine and terrestrial sterols and glycerol dialkyl glycerol tetraethers (GDGT). This is the first paleoclimatic application of IP25 in the Chukchi-Alaskan region of the Arctic, which is key for understanding Arctic-Pacific interactions and is experiencing rapid sea-ice retreat under present warming. Sea-ice and related circulation conditions were characterized in this study with a multi-century resolution for the long-term Holocene record to multi-decadal for the last several centuries. Sea ice was found to be present during the entire record, but with considerable spatial and temporal variability. After very low deglacial IP25 values, possibly related to permanent sea ice and/or an iceberg-dominated environment, cores from the upper slope and shelf show IP25 maxima, interpreted as representing a relative proximity to the sea-ice margin, in the early (ca. 8-9 ka) and middle (ca. 5-6 ka) Holocene, respectively. Along with isoprenoid GDGT distribution, this asynchronicity in sea-ice history probably reflects oceanographic evolution of the Chukchi margin affected by the Beaufort Gyre circulation and Pacific water inflow via Bering Strait. Data for the last several centuries, with elevated values of brassicasterol and terrestrial sterols co-varying with dinosterol and IP25, is interpreted in terms of long-distance import by currents combined with diagenetic transformations. We infer that high-amplitude variability in the late Little Ice Age, starting in the late 18th century, is related to the intensity of the Alaskan Coastal Current. This interval is preceded by three

	centuries of presumably diminished Alaskan Coastal Current, but overall increased Bering Strait Inflow resulting in reduced sea-ice cover according to dinocyst-based data.

Abstract

Two sediment cores from the Chukchi Sea margin were investigated for the Arctic sea ice biomarker IP_{25}, along with marine and terrestrial sterols and glycerol dialkyl glycerol tetraethers (GDGT). This is the first paleoclimatic application of IP_{25} in the Chukchi-Alaskan region of the Arctic, which is key for understanding Arctic-Pacific interactions and is experiencing rapid sea-ice retreat under present warming. Sea-ice and related circulation conditions were characterized in this study with a multi-century resolution for the long-term Holocene record to multi-decadal for the last several centuries. Sea ice was found to be present during the entire record, but with considerable spatial and temporal variability. After very low deglacial IP_{25} values, possibly related to permanent sea ice and/or an iceberg-dominated environment, cores from the upper slope and shelf show IP_{25} maxima, interpreted as representing a relative proximity to the sea-ice margin, in the early (ca. 8-9 ka) and middle (ca. 5-6 ka) Holocene, respectively. Along with isoprenoid GDGT distribution, this asynchronicity in sea-ice history probably reflects oceanographic evolution of the Chukchi margin affected by the Beaufort Gyre circulation and Pacific water inflow via Bering Strait. Data for the last several centuries, with elevated values of brassicasterol and terrestrial sterols co-varying with dinosterol and IP_{25}, is interpreted in terms of long-distance import by currents combined with diagenetic transformations. We infer that high-amplitude variability in the late Little Ice Age, starting in the late 18th century, is related to the intensity of the Alaskan Coastal Current. This interval is preceded by three centuries of presumably diminished Alaskan Coastal Current, but overall increased Bering Strait Inflow resulting in reduced sea-ice cover according to dinocyst-based data.

Keywords

Chukchi Sea, western Arctic, Holocene, sea-ice history, biomarker proxies, IP_{25}

Introduction

The Arctic is highly sensitive to the changing global climate due to powerful feedbacks collectively known as the Arctic Amplification (e.g., Miller et al., 2010). Sea ice plays a major role in these processes by largely controlling the surface albedo feedback. This setting justifies a high attention of the scientific community to the persistent Arctic sea-ice retreat that has been monitored for almost four decades (e.g., Stroeve et al., 2011). In addition to increases in downwelled longwave radiation and surface air temperatures, intensified advection of oceanic heat and changing atmospheric circulation patterns are identified as the main contributing factors to the ongoing sea-ice loss (Zhang et al., 2008; Woodgate et al., 2010). In particular, recent data indicate a critical role of the Pacific water influx for warming the western Arctic, where sea-ice retreat is most pronounced (Figure 1) (Shimada et al., 2006; Woodgate et al., 2010). Understanding the long-term behavior of these processes is complicated by the short duration of the instrumental record and the paucity of observations. For example, the transport of Pacific waters into the Arctic has only been measured directly for the last ~20 years (Woodgate et al., 2010).

Comprehending the development and consequences of the emerging new state of the Arctic with expanding swaths of open water requires a broad paleoclimatic perspective. The present interglacial (Holocene) covering the last approximately 12 ka, is a natural object for extended paleoclimatic research, especially considering the widespread availability of Holocene deposits (e.g., Miller et al., 2010; Polyak et al., 2010). Several studies emphasize the significance of the early Holocene (Holocene Thermal Maximum, HTM) for insights into the present Arctic warming and sea-ice shrinkage (e.g., Stranne et al., 2014), despite the differences in radiative forcing (insolation vs. atmospheric greenhouse composition) between these times. However, Arctic paleoclimate proxy data indicate a considerable geographic heterogeneity for the HTM. While most Arctic regions demonstrate a warming trend and diminished sea ice (e.g., Dyke and Savelle, 2001; Funder et al., 2011), some dinocyst-based reconstructions from the Chukchi margin, an area of pronounced modern sea-ice retreat, suggest the opposite pattern of sea ice growth during the HTM (de Vernal et al., 2008, 2013). One explanation for this anomalous picture infers atmospheric and oceanic circulation in the western Arctic that favors sea-ice build-up at the Chukchi margin, combined with enhanced ice formation on the adjacent shelves due to stronger seasonality. More studies, employing high-resolution records and various proxies, are therefore needed to delineate the Holocene history of the Chukchi region and its applicability for clarifying the long-term consequences of current climate change. In this paper, we investigate Holocene sea-ice conditions in two high-resolution sediment-core records from the northeastern (Alaskan) Chukchi Sea margin based primarily on the Arctic sea ice diatom biomarker IP_{25} (Belt et al., 2007), along with the concurrent analysis of some other biomarkers (marine and terrestrial sterols and glycerol dialkyl glycerol tetraethers) for further context. This study represents the first temporal application of IP_{25} from this region, which plays an important role in Arctic circulation and sea-ice regime.

Study area

The Chukchi Sea, connected to the Bering Sea via the narrow and shallow Bering Strait, acts as a distributor of water between the Arctic and Pacific oceans. The Bering Strait Inflow, an important carrier of heat and freshwater to the Arctic, transports the Pacific water to and across the Chukchi Sea in three major branches, which interact with the wind-driven Beaufort Gyre circulation at the Chukchi shelf margin (Figure 1) (e.g., Winsor and Chapman, 2004; Weingartner et al., 2005; Spall, 2007). The eastern branch forms the Alaskan Coastal Current, a buoyancy-driven boundary current along the Alaskan coast (Weingartner et al., 2005). The western branch flows northwestward, and can be especially strong, if easterly winds prevent the Alaskan Coastal Current (Winsor and Chapman, 2004). After crossing the Chukchi shelf, this branch, as well as the intermediate central branch, normally turns eastward along the shelf break (Spall, 2007). Under present conditions, thus, both the Alaskan Coastal Current and the recirculated western/central branches can affect the study sites.

Sea-ice conditions in the Chukchi Sea are strongly dependent on the wind patterns and the strength and distribution of the Bering Strait Inflow (Spall, 2007; Woodgate et al., 2010). Average spring-summer sea-ice concentrations in the late 20th century (climatological baseline) varied from ~50% near the Bering Strait to >90% at the northern margin of the Chukchi shelf, with the September ice margin (yearly minimum) well north of Alaska (Figure 1). In recent years, the margin of minimal sea-ice extent in this region has retreated considerably further north (Figure 1), with associated changes in the hydrography, primary production, and ecosystems (e.g., Grebmeier, 2012).

The Bering Strait Inflow and attendant circulation also controls sedimentary environments on the Chukchi shelf and slope. Fine sediments are largely re-suspended on the shallow, seasonally ice-free Chukchi shelf to be deposited on the northern slope and tributary canyons (Darby et al., 2009). The composition of these sediments may be affected by the circulation pattern and intensity. For example, some minerals associated with the North Pacific provenance, notably chlorite, can be used as a proxy of the Bering Strait Inflow (Ortiz et al., 2009; Nwaodua et al., 2014). Sedimentary organic matter can also bear evidence of the current impact as indicated by the distribution of terrestrial plant biomarkers, potentially related to the Yukon River runoff transported via the Bering Strait to the Chukchi-Alaskan margin (Goňi et al., 2013).

The Holocene history of circulation in the Chukchi Sea, as reconstructed from sediment core records, was initially controlled by the postglacial sea-level rise. The 40-50-m deep Bering Strait was inundated ca. 11-12 ka (Elias et al., 1992; Keigwin et al., 2006), but its complete availability for throughflow required another several ka. Based on proxy data, maximal Bering Strait Inflow effect on sedimentation at the northeastern Chukchi margin was reached by ca. 5-6 ka (Ortiz et al., 2009), consistent with the time of sea-level stabilization. Further evolution of the Bering Strait Inflow and related Chukchi Sea currents was likely controlled by atmospheric circulation, including the strength and position of the Aleutian Low (Danielson et al., 2014) and/or the inter-hemispheric wind stress (Ortiz et al., 2012).

IP_{25} and related biomarker proxy approach

The measurement of the IP_{25} biomarker in marine sediments has emerged as a powerful approach for paleo sea ice reconstruction in recent years (Belt et al., 2007; Belt and Müller, 2013). Amongst its properties, IP_{25} has been shown to be produced selectively by certain Arctic sea ice dwelling diatoms during the spring bloom and, upon ice melt, deposited in underlying sediments (Belt et al., 2007, 2013; Brown et al., 2011, 2014). As such, its sedimentary occurrence provides a relatively direct measure of the past occurrence of spring sea ice; an attribute not shared with other sea ice proxies such as planktonic micropaleontological assemblages. Currently, further work is needed to determine whether IP_{25}-based sea ice reconstruction can be made more quantitative; however it is noted that previous paleo sea ice reconstructions based on the presence and directional abundance changes of this biomarker are consistent with outcomes from other sea ice proxies or other oceanographic and climatic conditions (see Belt and Müller, 2013 for a review). Thus, the presence of IP_{25} in Arctic marine sediments provides evidence for the past occurrence of seasonal sea ice (Belt et al., 2007; Brown et al. 2011; Cabedo-Sanz et al., 2013), while changes in IP_{25} abundances track variability in sea-ice cover (e.g., Belt and Müller, 2013).

While being a robust indicator of sea-ice presence, IP_{25} does not show a straightforward relationship with sea-ice concentration or duration. The peak abundances of IP_{25} are expected to co-occur with sea-ice margin, from which IP_{25} values decrease towards both open water and permanent ice cover due to a likely reduced or even absent sea ice diatom growth (Müller et al., 2011; Belt and Müller, 2013). However, this pattern may be less clear in areas with a more patchy distribution of sea ice, without a well-expressed ice edge (Weckström et al., 2013). Distribution of IP_{25} in extended sea ice may also be more complex than initially thought. The early results indicated no detectable IP_{25} in sediments from the Canadian High Arctic with year-round ice cover (Belt at al., 2007). However, since this first report, analytical methods for identifying IP_{25} have improved, including further procedures that aid its detection at low concentration (Belt et al., 2012). In particular, IP_{25} has recently been reported in sediments from across the Arctic Ocean with permanent, or near-permanent sea ice cover (Xiao et al., 2015a). A potential solution to the interpretation of absent or very low IP_{25} is through the measurement of complementary biomarker signatures of open water conditions. An example of these is brassicasterol, a common lipid component in marine phytoplankton, whose abundance in sediments should also be sensitive to the overlying sea ice conditions. Thus, for low or absent IP_{25}, accompanying low brassicasterol might be expected under high ice cover, while high brassicasterol would more likely result from low sea ice or ice-free conditions. Further, Müller et al. (2011) showed that by combining concentrations of IP_{25} and brassicasterol (or other open-water indicators) into a single phytoplankton-IP_{25} index (PIP_{25}), it may be possible to obtain more quantitative estimates of sea ice conditions than from IP_{25} alone, and several applications of the PIP_{25} index for paleo sea ice reconstruction have appeared in recent years (e.g., Müller et al., 2012; Cabedo-Sanz et al., 2013; Stoynova et al., 2013; Xiao et al., 2015b). However, the assumptions and limitations associated with the use of the PIP_{25} approach have been discussed in detail by Belt and Müller (2013), and proponents of its use continue to emphasize that more work is needed to validate this approach.

The analysis of other biomarkers such as campesterol and β-sitosterol, believed to be derived mainly from terrestrial sources (higher plants), can provide information that is complementary to IP_{25} regarding oceanographic settings (Fahl and Stein, 2012 and references therein). Glycerol dialkyl glycerol tetraethers (GDGTs) also have the potential to provide relevant information, as marine production of isoprenoid GDGT can be affected by sea ice cover, while branched GDGT may help identify the provenance of organic matter, especially the input of terrestrial material from soils (Park et al., 2014 and references therein).

A detailed investigation of the distribution of IP_{25} has been performed in surface sediments of the southern Chukchi Sea, not quite reaching our study area (Stoynova et al., 2013). The IP_{25} distribution pattern shows a pronounced peak zone extending sub-latitudinally across the Chukchi shelf at ~70-72° N (pink field in Fig. 1). This zone corresponds to climatological average spring/summer sea-ice concentrations of 70-80% and is likely related to a stable ice edge occurring in early summer. A sharp southward decrease in IP_{25} values co-occurs with maximal concentrations of dinosterol, a biomarker of open-water conditions often proximal to sea ice. A comparable IP_{25} decrease north of the peak zone, towards more lasting sea-ice cover, has been documented west of the Chukchi Sea, but no samples were available to characterize this transition at the Alaskan margin. Yet further north, low IP_{25} values were found in the Canada Basin of the Arctic Ocean along with low concentrations of both brassicasterol and dinosterol, consistent with a lasting to permanent ice cover (Xiao et al., 2015a).

Material and methods

Sampling and age constraints

Sediment cores HLY0501-05TC/JPC and -08TC/JPC (trigger/ jumbo piston cores), hereafter referred to as 5JPC and 8JPC, were raised from the northeastern (Alaskan) margin of the Chukchi shelf in 2005 from the USCGC Healy (Figure 1) (Darby et al., 2005). Multicore 8MC raised nearby 8JPC was also used in this study. Core 8JPC is sited in the eastern part of the shelf, on the flank of the Barrow Canyon, a major conduit for water and sediment transport to the Alaska Beaufort margin and Canada Basin. Based on its relatively shallow water depth (90 m), the core site was exposed during the last glaciation and inundated during the postglacial transgression (e.g., Keigwin et al., 2006). In contrast, core 5JPC was raised from the continental slope at 415 m depth, where sediment deposition was not interrupted by sea-level changes.

Various stratigraphic, sedimentological, and geochemical data on these and nearby cores (Figure 1) have been reported in a number of papers (e.g., McKay et al., 2008; Darby et al., 2009, 2012; Lisé-Pronovost et al., 2009; Farmer et al., 2011; Faux et al., 2011). JPC to TC offsets due to overpenetration, which is especially common for JPC, were estimated from the comparison of various proxies, primarily measured continuously, such as bulk density, magnetic susceptibility, and diffuse spectral reflection (Darby et al., 2009). In addition, the 8MC to TC offset was estimated from data in this study. Sediments in most of 8JPC and ~13 m in 5JPC consist of bioturbated clayey silts indicative of marine environments (Darby et al., 2009), with a more sandy composition near the 8JPC bottom, possibly related to shallow-water erosion and re-deposition during shelf flooding. In 5JPC, the homogenous, fine-grained marine unit is underlain by a more complex lithostratigraphy with laminations and coarse ice-rafted debris indicative of glaciomarine environments affected by glacial/deglacial processes (McKay et al., 2008; Polyak et al., 2009). Organic carbon content shows a steep increase from below 1% in the upper part of the deglacial unit to nearly 1.5% in the lower Holocene and then a slight, gradual increase towards the core top with only minor variability (Figure 2; McKay et al., 2008; Curry, 2009; Faux et al., 2011). A previous study of organic markers in 5JPC indicates predominantly marine sources of organic matter in the Holocene with lower but continual contributions from terrestrial sources (Faux et al., 2011), consistent with data from surficial sediments at the Chukchi margin (Belicka et al., 2004).

206 Age constraints were provided by six and ten accelerator mass spectrometry (AMS) ^{14}C
207 ages of mollusc shells from cores 5JPC and 8TC/JPC, respectively (Figure 2; Suppl. 1) (Darby et
208 al., 2009), with concurrent age controls from paleomagnetic data (Lisé-Pronovost et al., 2009)
209 and ^{210}Pb in the upper part of 5TC (McKay et al., 2008). ^{14}C ages were converted to calendar
210 ages using the CALIB7.0 program and marine13 dataset (Reimer et al., 2013). Local reservoir
211 corrections (ΔR) were taken as 500 years for 8JPC washed by surface waters with a strong
212 Pacific component and 0 years for 5JPC washed by subsurface Atlantic waters below 200 m
213 (McNeely et al., 2006; Darby et al., 2012). We note that the actual ΔR values in the study area
214 may have varied during the Holocene, especially at shallower sites, due to changes in sea level
215 and hydrographic structure.

216 The age model, except for 5TC, was constructed by linear interpolation between the ^{14}C
217 datings, which fall within the interval of ca. 2.4–7.7 cal ka, as well as the assumed modern age of
218 the 5TC and 8MC tops. The best ^{14}C-based age control covers the interval of 4.1-7.3 ka in 8JPC
219 and 4.7-6.9 ka in 5JPC. Ages below the dated ranges were extrapolated to the bottom of the
220 Holocene marine unit but, in 8JPC, this estimate was complicated by an age inversion in the
221 lower part of the core (Figure 2), reflected in two age models below this level (solid and dashed
222 lines in Figure 3). The resulting age of the marine unit bottom differs between the two cores by
223 one to nearly two ka (depending on the choice of the lowermost dating used in 8JPC), which
224 could be an artifact of extrapolation and/or a true asynchroneity related to different water depths.
225 Age constraints for glacial/deglacial sediments in 5TC were estimated using lithological tie
226 points from the regional stratigraphic context, such as the bottom of iceberg-rafted deposits and
227 the onset of sediment transport from the Bering Strait (Polyak et al., 2009). The distribution of
228 linear sedimentation rates in the Holocene marine unit shows maximal values in both cores

around 5-6 ka, with especially high rates attained in 8JPC. The age model for 5TC was estimated from ^{210}Pb data measured in the upper 15 cm (McKay et al., 2008). Although we cannot guarantee a robust extrapolation of sedimentation rates from the analyzed interval to the entire ~2.5-m-long 5TC, we use this approach as no ^{14}C age has been obtained from this core. Bioturbation in the Arctic Ocean and specifically in the study area has been estimated as modest, e.g., 2-3 cm at water depths >150 m and somewhat higher at shallower depths (Clough et al., 1997; Pirtle-Levy et al., 2009), and is therefore unlikely to have a strong effect on the age model, especially in 5TC/JPC.

A total of 62 and 49 samples were collected for IP_{25} analysis from cores 5TC/JPC and 8MC/TC/JPC, respectively; 37 and 32 of them were also analyzed for marine/terrestrial sterols. Isoprenoid GDGT data cover 47 and 34 samples from the same cores as part of a broader GDGT study. Samples were mostly taken from the Holocene marine sediments at intervals intended to provide a multicentury-scale resolution (~200-400 years per sample at most of the record length). The uppermost part of the cores (~0.5 m of composite core depth) was sampled for IP_{25} at higher resolution, up to 10-20 years per sample in 5TC, in order to characterize the most recent record in more detail. In addition, several samples from the lower part of 5JPC span the deglacial sedimentary sequence. Samples were stored in a refrigerator following collection, then sub-sampled and freeze-dried for further processing.

Biomarker analysis

IP_{25} and sterols were analyzed following methods described previously (Brown et al., 2011; Belt et al., 2012). Briefly, 9-octylheptadec-8-ene (9-OHD, 10 µL; 10 µg mL^{-1}) and 5α-androstan-3β-ol (10 µL; 10 µg mL^{-1}) were added to ca. 1 – 2 g of each freeze-dried sediment sample prior to extraction to permit quantification of IP_{25} and sterols, respectively. Samples were then extracted using dichloromethane/methanol (3 x 3 mL; 2:1 v/v; ultrasonication; 15 min), centrifuged (2500 rpm; 1 min) and dried (N_2). The resulting dried total organic extracts (TOE) were dissolved in hexane (ca. 1 mL) and purified using column chromatography (silica) with IP_{25} (hexane; 6 mL) and sterols (20:80 methylacetate/hexane; 6 mL) collected as two single fractions. Analysis of individual fractions was carried out using gas chromatography - mass spectrometry (GC-MS) with operating conditions as described previously (Belt et al., 2012). Sterols were derivatized (BSTFA; 50 µL; 70 ºC; 1 h) prior to analysis by GC-MS. Mass spectrometric analysis was carried out in total ion current (TIC) and single-ion monitoring (SIM) modes. Individual lipids were identified on the basis of their characteristic GC retention indices and mass spectra obtained from standards. Quantification of IP_{25} was achieved by dividing its integrated GC-MS peak area by that of the internal standard (9-OHD) in SIM mode (both *m/z* 350) and normalising this ratio using an instrumental response factor (obtained from laboratory standards of each analyte) and the mass of sediment (Belt et al., 2012). Analytical reproducibility (5 %, n = 4) was monitored using homogenized sediment material with a known concentration of IP_{25}, similar to those found for the sediments under study (Belt et al., 2012). Values were further checked through analysis of this homogenized sediment for every 8–12 sediment samples extracted, as per the recommendation of Belt et al. (2012). Sterol concentrations were obtained by comparison of their respective peak areas in SIM mode (brassicasterol, *m/z* 470; campesterol, *m/z* 382; dinosterol, *m/z* 500 and β-sitosterol, *m/z* 396) with those of the internal standard (*m/z* 333) and normalized as per IP_{25}. Since we did not have a laboratory standard of dinsoterol, we determined its instrumental response factor by analysis of sediment with known concentration (Faux et al., 2011). P_BIP_{25} and P_DIP_{25} values were determined from IP_{25} and brassicasterol or dinosterol data according to the method of Müller et al. (2011). Biomarker concentrations were also combined with dry bulk densities and expressed in μg/cm^3 to account for changes in sediment density (Belt et al., 2012). Due to a relative sparsity and uneven downcore distribution of age control points we prefer not to express IP_{25} data as annual fluxes as done in some studies (Müller et al., 2009; Vare et al., 2009; Belt et al. 2010).

GDGTs were analyzed as described in Park et al. (2014), using the recommended methodical guidelines of Hopmans et al. (2000), Huguet et al. (2006), and Schouten et al. (2007).

Results

IP_{25} concentrations in core 5TC/JPC range from nearly 0 to 0.025 μg/cm^3 of dry sediment (Figures 2-3). Despite overall low values, all samples in the deglacial/Holocene sediments have non-zero IP_{25} concentrations. One sample analyzed from the bottom-most unit, presumably deposited during the glacial maximum (beyond the stratigraphic range in Figure 3), did not show detectable levels of IP_{25}. In most of the deglacial section until estimated 11 ka, IP_{25} values stay very low, then increase to ~0.02 μg/cm^3 towards the bottom of the marine unit, and gradually decrease from ca. 8.5 to 6.5 ka. In the remainder of the middle to late Holocene, IP_{25} levels remain low, around 0.01 μg/cm^3, but get somewhat higher at ca. 1 ka and, especially, within the last two centuries.

In core 8MC/TC/JPC, IP_{25} concentrations are similar to those in 5JPC, with overall slightly higher values of ~0.01 to 0.035 μg/cm^3, but the downcore distribution differs considerably (Figures 2-3). In the lower to middle Holocene, maximum IP_{25} values occur in the interval ca. 5-7 ka, with the highest levels attained between 5 and 6 ka, and overall lower values below and above this interval. In the late Holocene, IP_{25} values in 8JPC are still higher than in 5JPC, and especially high, although variable, in the last millennium. We note that the analyzed 8JPC record does not extend below the marine Holocene unit, where sedimentation was probably predominated by shallow-water processes.

Downcore distribution of dinosterol is generally similar to that of IP_{25} in both cores (Figure 2). Brassicasterol shows a similar pattern between the cores, with a distribution alike IP_{25} in 5JPC, but not in 8JPC. It is also distributed similarly to terrestrial sterols, with a five-fold increase in both cores at the subsurface interval corresponding to the last four-five centuries. To account for this increase in sterol concentrations, the balance factor for the PIP_{25} indices derived from IP_{25} and brassicasterol or dinosterol data was calculated for the subsurface interval and the rest of the stratigraphy separately (see more discussion below).

Concentrations of isoprenoid GDGT in both 5JPC and 8JPC have low to moderate values under ~18 μg/g (Figure 3). In the late deglacial interval to the early Holocene (until ca. 9 ka), concentrations are low in both cores, then increase markedly in 5JPC to a maximum around ca. 5–6 ka. Later in the Holocene, isoprenoid GDGT values are overall high, but variable. Similar GDGT distribution characterizes core ARA-03B GC01 further west on the Chukchi shelf (Figure 1) (Park, pers comm). In contrast, in 8JPC, isoprenoid GDGT concentrations exhibit a distinct maximum around ca. 3 ka. The branched and isoprenoid tetraether (BIT) index is high in deglacial sediments in 5JPC and decreases in both cores to very low values after ca. 8 ka in 5JPC and two ka later in 8JPC (Figure 3).

Discussion

Background interpretation of the observed biomarker distributions

Concentrations of IP_{25} in the Holocene record of both cores under study, when normalized to organic carbon, constitute mostly ~1-2 µg/g OC, an order of magnitude lower than peak values identified in surface sediments of the Chukchi shelf further south (Stoynova et al., 2013) but comparable to values found north of the study area (Xiao et al., 2015a). It must be noted, however, that the IP_{25} data reported by Stoynova et al. (2013) appear to have an offset from the other Arctic data sets, possibly attributed to inter-laboratory calibration issues (Xiao et al., 2015), so the difference of our IP_{25} values from those of Stoynova et al. (2013) may not be that large. In any case, although low, these values along with attendant concentrations of brassicasterol and dinosterol equivalent mostly to ~5-20 µg/g OC (higher brassicasterol in the youngest sediment) fall within the range deemed useful for characterizing Arctic sea-ice conditions (Müller et al., 2011; Xiao et al., 2015a). Together with P_BIP_{25} and P_DIP_{25} indices averaging between ~0.3 to 0.6 at most of the core length in 5JPC and slightly higher in 8JPC, the observed IP_{25} values correspond to the conditions of marginal ice zone to extended ice cover common for the northern edge of the Arctic continental margin (Xiao et al., 2015a). We note that even lower values of IP_{25} have also been used for reconstructing paleo-sea-ice conditions in the Arctic Ocean (Xiao et al., 2015b).

Slightly higher concentrations of IP_{25} as well as PIP_{25} indices at most of the core length in 8JPC might indicate that this site was overall closer to the sea-ice margin than 5JPC. However, biomarker concentrations can have site specific differences, as exemplified by the CAA cores that have very different average IP_{25} values despite coherent temporal patterns (Belt et al., 2010). Therefore, we base our interpretation primarily on down-core changes in IP_{25}, which are considerably different between JPC5 and JPC8 at most of the record (Figure 2-3). This pattern is shared by dinosterol to some extent, whereas brassicasterol and terrestrial sterols have a more comparable distribution in both cores, with a concerted steep increase followed by a large variability in the upper part of the record. Cross-plotting of brassicasterol vs. terrigenous sterol concentrations (Figure 4) confirms their close relationship, especially evident in the upper part of the cores (last four-five centuries), where concentrations are overall higher and vary within a broad range. Dinosterol and IP_{25} also show a relationship with brassicasterol in this interval but without a corresponding increase in their concentrations, which makes this youngest record notably different from the rest of the stratigraphy.

The close relationship of markers from different sources is unusual and indicates an impact from an external factor such as a dilution by mineral sediment matrix or a co-delivery to the core sites by the same transportation mechanism. As mineral dilution in the upper part of the cores is unlikely, due to a lack of co-variation of the sterol data with the total organic carbon content (Figure 2), we infer that delivery of both marine and terrestrial components by ocean currents provides a likely explanation. In support of this, we note that the study sites are affected by cross-shelf currents originating from the North Pacific, notably by the Alaskan Coastal Current that has an especially strong influence on 8JPC (Figure 1). The Alaskan Coastal Current carries fines from the coastal areas of the eastern Bering Sea encompassing sites with high marine organic production and the estuarine areas including the large Yukon River, and can therefore provide an effective transport mechanism for both marine and terrestrial organic markers. Indeed, the relationship between brassicasterol and IP_{25} in the broad regional context

(Figure 5) shows that data from the younger record in cores under study falls between the Chukchi shelf and the North Pacific signature, thus indicating the likelihood of long-distance sediment transport. In comparison, data from the older record shows more affinity to the Chukchi shelf sediments, suggesting the prevalence of more local processes during most of the Holocene. Elevated concentrations of brassicasterol and terrestrial sterols in the subsurface record could also be controlled by diagenetic transformation, but this, alone, cannot adequately explain the observed high variability in biomarker values (more discussion in the last section below). Regardless of the exact mechanism, we infer that interpretation of the youngest record (last four-five centuries) is likely to be biased by long-distance sedimentary inputs, possibly in combination with some diagenetic changes. In contrast, the rest of the stratigraphy under study may be more suitable for reconstruction of local sea-ice conditions. We note that the range of our Holocene data could be even closer to the recent Chukchi Sea IP_{25} values of Stoynova et al. (2013), due to a potential inter-laboratory data offset, as suggested by Xiao et al. (2015a).

A dual application of biomarker and transfer functions based on, e.g., dinosysts, which consistently occur in Arctic Holocene sediments, offers a potentially promising approach to sea-ice reconstructions. However, a comparison between IP_{25} and dinocyst-based reconstructions of sea-ice conditions in 5JPC shows a mixed picture of consistent patterns at some intervals, but a considerable divergence at others (Figure 3). Overall, the dinocyst data show more variability compared to the biomarker record. There is currently no consensus on why outcomes derived from these two sea ice proxies should be different (Belt and Müller, 2013). Apparent inconsistencies in temporal sea ice profiles may better reflect differences between the precise signatory natures of the individual proxies themselves, rather than anomalies. Thus, peaks in IP_{25} are believed to reflect primarily spring/summer sea ice edge (Müller et al., 2011; Belt and

Müller, 2013), whereas dinocyst reconstructions are related to a longer-term, annual perspective (i.e., months/yr cover) (e.g., de Vernal et al., 2008). The inter-relationships that may exist between the two approaches are, thus, in need of further attention. Nevertheless, what is clear from application of both approaches to the Alaskan margin sites, is the pervasive occurrence of sea ice cover throughout the Holocene.

Long-term Holocene record

Interpretation of extremely low IP_{25} concentrations in the deglacial record, exemplified by the lower part of 5JPC (Figures 2-3), is not straightforward. One possibility is that low IP_{25} values along with low brassicasterol and dinosterol concentrations identified for the top of this interval reflect permanent sea-ice cover such as in the Canada Basin in recent conditions (Xiao et al., 2015a). The paleogeographic setting at the Chukchi margin during deglaciation was also potentially amenable for sea-ice build-up due to meltwater inputs from the retreating Laurentide Ice Sheet and a not fully open Bering Strait. On the other hand, the deglacial environment was affected by strong iceberg discharge, as indicated by the high content of coarse debris including rocks with the Laurentide provenance (Darby et al., 2001; McKay et al., 2008; Polyak et al., 2009). The imported nature of the deglacial sediment is further corroborated by a high content of branched GDGT (BIT index; Figure 3) that is indicative of enhanced delivery of terrestrial (soil) organic material (Hopmans et al., 2004). Numerous icebergs likely disrupt the "normal" development of sea-ice cover and the formation of ice-related biotic assemblages, which could result in very low IP_{25} and spurious PIP_{25} values. In addition, sedimentation overwhelmed by terrigenous material delivered by icebergs and meltwater further reduces IP_{25} concentrations. For a comparison, Alonso-Garcia et al. (2013) showed that high content of coarse debris resulting from rapid discharges of icebergs coincided with relatively low IP_{25} concentrations in sediment from the East Greenland Shelf during the 2nd half of the 19th century despite relatively high ice conditions overall.

Regardless of the interpretation of deglacial sea-ice conditions, a conspicuous increase in IP_{25}, along with dinosterol, with a transition to the marine Holocene unit (Figures 2-3) likely indicates an increasing proximity of the sea-ice margin. An accompanying increase in brassicasterol, however, should be considered with caution as a similar pattern in 8JPC is not coupled with changes in IP_{25}. The brassicasterol profile in both cores is comparable to that of terrestrial plant sterols, with a slight offset in the position of peak values in the lower Holocene, and could be thus related to an increasing long-distance advection via the widening Bering Strait. A further decrease of sterol concentrations may indicate a subsided advection to the study sites, possibly due to circulation changes, combined with reduced local phytoplankton production.

A notable feature in the observed IP_{25} distribution in the marine unit is the difference between the two cores, with a broad maximum in the early Holocene (from estimated 10-11 ka to ca. 6.5-7 ka) in 5JPC vs. the delayed maximum at 5-7 ka in 8JPC that corresponds to especially high IP_{25} fluxes considering high sedimentation rates during this time interval exceeding 1 m/ka (1 mm/a) around ca. 5 ka (Figure 3). Changes in PIP_{25} indices generally follow this pattern, especially consistent for P_DIP_{25} in 5JPC. Provided these changes represent mostly local conditions, the decrease in IP_{25} and PIP_{25} after ca. 8 ka in 5JPC and ca. 5 ka in 8JPC may indicate an overall reduction in the duration of ice cover. A comparison with GDGT distribution shows that concentrations of isoprenoid GDGT in both cores increased after the decline of IP_{25}, peaking at ca. 5−6 ka in 5JPC and around ca. 3 ka in 8JPC. This delay of isoprenoid GDGT relative to IP_{25} is consistent with the inferred negative effect of sea ice on local GDGT production (Park et al., 2014), while the temporal shift between isoprenoid GDGT maxima underscores the asynchronicity in sea-ice conditions across the Chukchi margin as expressed in IP_{25} records.

Sedimentary factors may have a considerable effect on the distribution of organic matter and its constituents in sediments at the Chukchi margin by controlling transportation, redistribution, and deposition of fines (Darby et al., 2009). Faux et al. (2011) have concluded that Holocene sediments in 5JPC were mostly well mixed prior to deposition. However, sedimentary factors are unlikely to play a significant role in the observed asynchronous pattern of biomarker distribution between 5JPC and 8JPC as maximal sedimentation rates, and thus maximal resuspension of fines on the Chukchi shelf, occur at about the same time (ca. 5-6 ka) in both cores (Figure 3). A more plausible explanation is related to circulation changes, such as the distribution of Bering Strait Inflow water between different branches and strength of the Beaufort Gyre (Figure 6).

The early Holocene pattern of biomarker distribution at the Chukchi margin, exemplified primarily by 5JPC, is more difficult to interpret due to non-analog conditions related to an incompletely open Bering Strait and potentially lingering meltwater. Nevertheless, a pronounced peak of IP_{25} and relatively high PIP_{25} values in 5JPC indicate an overall significant presence of sea ice in this area, consistent with an earlier conclusion based on dinocyst assemblages (de Vernal et al., 2008, 2013). This conclusion contrasts an inferred early-Holocene ice retreat in other parts of the Arctic Ocean periphery, notably north of Greenland and the Canadian Arctic (Dyke and Savelle, 2001; Funder et al., 2011). This contrast is illustrated further by a comparison of IP_{25} records from the Chukchi margin and the straits of the Canadian Arctic Archipelago (CAA) (Figure 7; Vare et al., 2009; Belt et al., 2010). The early Holocene IP_{25} maximum in 5JPC has no counterpart in any of the CAA cores, while for the easternmost location (core 3), this interval has minimal IP_{25} values, interpreted to represent the lowest sea-ice occurrence (Vare et al., 2009). A possible reason for anomalously extended ice cover at the Chukhi-Alaskan margin in the lower Holocene might be related to insufficient advection of warm waters via the Bering Strait (Figure 6a) and intensified import of ice by the Beaufort Gyre. Indeed, mineral provenance records indicate increased transport of sediment by way of the Beaufort Gyre at that time (Yamamoto, pers. comm.), possibly due to its mobility provided by melting sea-ice at the margins under overall warmer climatic conditions, similar to the intensified Beaufort Gyre movement in recent decades (Shimada et al., 2006).

The delayed IP_{25} peak in 8JPC occurred at a time when the Bering Strait Inflow reached its maximum in the middle Holocene (between ca. 6 and 4 ka) as indicated by a sediment provenance proxy record proximal to 5JPC (Ortiz et al., 2009) and confirmed, further, by data from a more westwards core GC01 (Fig. 1; Yamamoto, pers comm). This maximal inflow is also reflected by peak sedimentation rates at the Chukchi margin (Figure 3) due to intense re-suspension and deposition of fine sediment (Darby et al., 2009). High Bering Strait Inflow volumes favor westward diversion of more Pacific water at the expense of diminished Alaskan Coastal Current contribution (Winsor and Chapman, 2004), which is consistent with our inference of sea-ice retreat at the 5JPC site, but higher ice coverage in 8JPC further east (Figure 6b). A comparison with the IP_{25} records from the CAA shows that sea-ice expansion by way of the Alaskan Coastal Current may have affected the proximal part of the CAA straits (i.e. cores 4 and 5), but not the eastern area exemplified by core 3 (Figs. 1, 7). After ca. 4 ka, the strength of the Bering Strait Inflow decreased, probably driven by changes in atmospheric circulation (Ortiz et al., 2009, 2012), resulting in a more equitable distribution of Pacific water between western and eastern branches, and thus, of sea-ice extent (Figure 6c). Based on higher IP_{25} values in 8JPC, ice conditions were probably more severe, overall, in the eastern area. It is also possible that summer sea ice distribution in the northern Chukchi Sea was irregular, due to a relatively sluggish circulation; a pattern consistent with historical observations and related modeling (Spall, 2007). A prominent IP_{25} peak at ca. 2-2.5 ca in the eastern CAA core 3, possibly representing Neoglacial cooling (Figure 7; Vare et al., 2009), is absent both in the Chukchi and western CAA cores.

Last millennium

A notable pattern in IP_{25} and sterol data in the record corresponding to the last several centuries requires further discussion, especially considering the heightened relevance of this time interval for comparison with modern natural climatic conditions. Overall low and stable sterol values in most of the Holocene record show a pronounced increase in variability, along with concentrations of brassicasterol and terrestrial sterols, in the last four-five centuries, according to the existing age models based on ^{210}Pb data in 5TC (McKay et al., 2008) and ^{14}C interpolation in 8MC/TC (Figures 2, 8). IP_{25} values in this interval exhibit a similar variability, without an increase relative to the peak values in the older Holocene record. As discussed above, the co-variation including the concerted rise in both marine (brassicasterol) and terrigenous (higher plants) sterols in the recent sediments may be related to diagenetic processes, long-distance co-delivery by currents, or a combination of these factors.

Diagenetic degradation of organic matter is expected in subsurface marine sediments, including the Arctic seas, and can affect all organic constituents, although likely at different rates (e.g., Harvey et al., 1986; Haddad et al., 1992; Belicka et al., 2004; Goňi et al., 2013). The apparent lower (or absent) diagenetic loss of dinosterol in our data could be related to a lower reactivity compared to other sterols, especially since the former does not contain a ring double bond found in all Δ^5 sterols (e.g. brassicasterol), and which plays a key role in abiotic sterol degradation reactions including photo- and autoxidation (Christodoulou et al., 2009; Rontani et al., 2009). This inference is also consistent with data from subsurface records in the western Arctic indicating generally only subtle downcore diagenetic changes in biomarker distributions including dinosterol (Belicka et al., 2004). While diagenetic reactivity of different biomarkers requires further investigation, the high variability in the record under discussion cannot be explained by organic matter degradation alone; neither can it be attributed to the impact of burrowing organisms, which appears to affect only a few upper centimeters in sediments throughout the study region (Clough et al., 1997; Pirtle-Levy et al., 2009). This indicates that the observed variability in sterol and IP_{25} concentrations is likely related to changes in circulation, while an overall downcore decrease in concentrations of some biomarkers could be controlled by diagenetic losses. In order to obtain a clearer picture of the inferred current-related variability, the profiles of brassicasterol and terrestrial sterols have been quadratically detrended (Figure 8).

Interestingly, the sharp rise in terrestrial sterols is not accompanied by a comparable increase in branched GDGT (BIT index) (Figure 3), which indicates a likely different provenance of imported terrestrial material. In the deglacial time and early Holocene it was mostly represented by soil-derived organic matter, probably originating from the melting of Laurentide ice and/or the Mackenzie River. In contrast, in the last centuries, terrestrial material was related largely to higher plant debris that is not common for high-Arctic river load and is more likely transported from the Yukon River by way of the Alaskan Coastal Current. This provenance interpretation is consistent with biomarker distributions in modern sediments from the Chukchi-Alaskan margin and the Mackenzie area (Goňi et al., 2013).

Reconstructions of sea-ice cover duration based on dinocyst assemblages from 5TC and a box core B5 further north (Figure1) indicate overall less ice during the late 15th to late 18th century AD, before a subsequent expansion of sea-ice cover in the late Little Ice Age (LIA) (Figure 8; de Vernal et al., 2008; Farmer et al., 2011). A generally similar pattern can be seen in several proxy records around the Arctic Ocean and in a pan-Arctic millennial sea-ice synthesis based on these records, including B5 (Kinnard et al., 2011). While the pan-Arctic record can be affected by multiple factors including the North Pacific and, especially, North Atlantic climatic variability (Kinnard et al., 2011), the Chukchi region has more affinity to the North Pacific atmospheric and oceanic circulation. In particular, the strength and position of the Aleutian Low pressure system largely controls the Bering Strait Inflow, and thus sea-ice conditions in the Chukchi Sea (Danielson et al., 2014). While no long-term proxy record exists strictly for the Aleutian Low, several paleoclimatic studies from the Northwest Pacific region provide relevant information. A strong westerly Aleutian Low, which enhances Bering Strait Inflow, is consistently indicated by ice cores from southern Alaska (Fisher et al., 2008; Porter, 2013) and lake records from the Alaskan interior (Gonyo et al., 2012 and references therein) for the 16th to 18th century, the time of reduced sea ice at the Chukchi margin according to dinocyst-based reconstructions (de Vernal et al., 2008; Farmer et al., 2011). This circulation setting, however, negatively affects the Alaskan Coastal Current that delivers warm water and sediment load to the northeastern Chukchi Sea and further downstream along the northern Alaskan coast (Winsor and Chapman, 2004). In contrast, the more easterly/weaker Aleutian Low in the late LIA favored more ice cover developed in the main Chukchi Sea, but stronger Alaskan Coastal Current, which increased the delivery of sediment load to the northeastern area. This circulation history appears consistent with overall anomalously high and variable sterol and co-varying IP_{25} values in the record under study corresponding to the late LIA, and relatively depressed values in the preceding three centuries (Figure 8). It is unclear, to what extent IP_{25} values reflect local sea-ice conditions, but a strong co-variation with sterols that were likely imported from a long distance, suggest a mostly external source for IP_{25} as well.

The circulation history inferred for the last millennium, with principally two alternating regimes of the Bering Strait Inflow, appears similar to the interpretation of longer-term changes in the lower and middle Holocene, as discussed above (Figure 6). However, many of the conditions earlier in the Holocene were not quite analogous to the more recent situation. These include a different configuration of the Bering Strait, a lingering Laurentide ice sheet that strongly affected the atmospheric circulation (e.g., Kaufman et al., 2004) and potentially other climatic and oceanographic factors. These non-analog conditions may have caused the differences between patterns in the earlier record and in the last several centuries, such as an explicitly asynchronous distribution of IP_{25} between the study sites and mostly uniformly low brassicasterol and terrestrial sterol concentrations in the early to middle Holocene.

We speculate further that shorter-term variability, expressed especially in the uppermost part of a densely sampled 5TC (Figure 8), reflects major fluctuations in the Alaskan Coastal Current linked to a documented multi-decadal variability in the Aleutian Low (e.g., Hetzinger et al., 2012), although this inference requires more detailed studies on high-resolution cores from the Chukchi-Alaskan margin. The reason for a contrast between a variable LIA and relatively monotonous earlier biomarker record, especially apparent in 5 TC (Figure 8), is also not clear from the existing data as the sampling points below the late LIA record are not that sparse to miss fluctuations in the data measured altogether. A more pronounced amplitude in sterol and IP_{25} variations in the late LIA could be accentuated by diagenetic degradation downcore that makes earlier variability less discernable, but the question remains, whether this amplitude change also has a paleoclimatic significance. Anomalously high-amplitude variability in the late LIA is not apparent in related proxy records from other Arctic/subarctic regions, except for an IP_{25} dataset north of Iceland that does not, however, extend far beyond the last millennium (Massé et al., 2008). On the other hand, a millennial tree-ring record of the Pacific Decadal Oscillation, which is linked with the Aleutian Low history, suggests that a strong, persistent decadal to multi-decadal variability is only characteristic for the last two centuries (MacDonald and Case, 2005).

A comparison with the CAA data shows a pronounced rise in IP_{25} in the early LIA in cores 4 and 5, but not in the eastern core 3 (Figures 7-8; Belt et al., 2010), indicating an extended sea-ice cover in the western CAA, possibly related to a restricted Alaskan Coastal Current. However, a comparison with core 3 may be inconclusive as it lacks sediment from the last five centuries according to the age model applied (Vare et al., 2009).

Conclusions

This study provides the first paleoclimatic application of IP_{25} and related biomarkers for evaluating the Holocene sea-ice history in the Chukchi-Alaskan region of the Arctic Ocean, which plays a critical role in Arctic-Pacific interactions and is currently experiencing a dramatic retreat of sea ice under present warming. The long-term record investigated in two sediment cores, mostly at multi-century time scale, indicates an overall persistent presence of sea ice throughout the Holocene, but with considerable spatial and temporal variabilities. The pre-Holocene (deglacial) record from the Chukchi margin has very low IP_{25} values, probably related to some combination of sea ice and iceberg-bearing environments. An IP_{25} maximum around 8-9 ka in a core from the shelf break suggests expanded sea ice in the western Arctic Ocean despite the early Holocene warming, consistent with some earlier dinocyst-based reconstructions (de Vernal et al., 2008, 2013). In a core further southeast, peak IP_{25} values, presumably characterizing a relative proximity to sea-ice margin, were reached ~3 ka later. In both cores, isoprenoid GDGT have maximum concentrations with an ~1-2 ka delay relative to IP_{25}, probably signifying sea-ice retreat. The asynchronous development of sea ice at these sites may be related to circulation history such as an undeveloped Bering Strait Inflow and, possibly, a stronger Beaufort Gyre in the early Holocene, and a higher, westward deflected Bering Strait Inflow in the middle Holocene.

The biomarker record for the last several centuries demonstrates a strong temporal variability along with overall elevated values of brassicasterol and terrestrial sterols. This anomalous increase in biomarker concentrations is interpreted in terms of long-distance import by currents combined with diagenetic transformations. Although probably not representing local sea-ice conditions, this record may have value for characterizing broader circulation patterns. In particular, we infer that high-amplitude variability in the late Little Ice Age, starting in the late 18th century, is related to the intensity of the Alaskan Coastal Current. This interval is preceded by three centuries of presumably diminished Alaskan Coastal Current, but overall increased Bering Strait Inflow resulting in reduced sea-ice cover according to dinocyst-based data (de Vernal et al., 2008; Farmer et al., 2011).

Results of this study offer further opportunities to investigate linkages between atmospheric and oceanic processes in the Arctic-Pacific region on various time scales. The data obtained also highlight a need to resolve differences between individual proxies, such as IP_{25} and dinocyst assemblages. Emphasis should therefore be put on a multi-proxy approach to sediment cores, with high temporal resolution from locations representing key circulation and sea-ice features.

Supplementary data to this contribution can be found online alongside the full-text article.

Acknowledgments

This work was partially supported by the US National Science Foundation award ARC-1304755 to LP. SB and PCS thank the University of Plymouth for financial support and to John Price for carrying out preliminary IP_{25} measurements. The GDGT study was supported by a grant-in-aid for Scientific Research (B) from the Japan Society for the Promotion of Science, No. 25287136, to MY. We thank two anonymous reviewers for insightful comments that helped to improve the manuscript.

References

Alonso-García M, Andrews JT, Belt ST et al. (2013) A comparison between multi-proxy and historical data (AD 1990-1840) of drift-ice conditions on the East Greenland shelf (~66°N). *The Holocene* 23: 1672–1683.

Belicka LL, Macdonald RW, Yunker MB and Harvey HR (2004) The role of depositional regime on carbon transport and preservation in Arctic Ocean sediments. *Marine Chemistry* 86: 65–88.

Belt ST, Masse G, Rowland SJ et al. (2007) A novel chemical fossil of palaeo sea ice: IP25. *Organic Geochemistry* 38: 16–27.

Belt ST, Vare LL, Masse G et al. (2010) Striking similarities in temporal changes to spring sea ice occurrence across the central Canadian Arctic Archipelago over the last 7000 years. *Quaternary Science Reviews* 29: 3489–3504.

Belt ST, Brown TA, Navarro Rodriguez A et al. (2012) A reproducible method for the extraction, identification and quantification of the Arctic sea ice proxy IP_{25} from marine sediments. *Analytical Methods* 4: 705–713.

Belt ST, Brown TA, Ringrose AE et al. (2013) Quantitative measurements of the sea ice diatom biomarker IP_{25} and sterols in Arctic sea ice and underlying sediments: Further considerations for palaeo sea ice reconstructions. *Organic Geochemistry* 62: 33–45.

Belt ST and Müller J (2013) The Arctic sea ice biomarker IP_{25}: a review of current understanding, recommendations for future research and applications in palaeo sea ice reconstructions. *Quaternary Science Reviews* 79: 9–25.

Brown TA, Belt ST, Mundy C et al. (2011) Temporal and vertical variations of lipid biomarkers during a bottom ice diatom bloom in the Canadian Beaufort Sea: further evidence for the use of the IP_{25} biomarker as a proxy for spring Arctic sea ice. *Polar Biology* 34: 1857–1868.

Brown TA, Belt ST, Tatarek A and Mundy CJ (2014) Source identification of the Arctic sea ice proxy IP_{25}. *Nature Communications* 5: 4197.

Cabedo-Sanz P, Belt ST, Knies J and Husum K (2013) Identification of contrasting seasonal sea ice conditions during the Younger Dryas. *Quaternary Science Reviews* 79: 74–86.

Christodoulou S, Marty J-C, Miquel J-C et al. (2009) Use of lipids and their degradation products as biomarkers for carbon cycling in the northwestern Mediterranean Sea. *Marine Chemistry* 113: 25–40.

Clough LM, Ambrose WG, Cochran JK et al. (1997) Infaunal density, biomass and bioturbation in the sediments of the Arctic Ocean. *Deep-Sea Research II* 44: 1683–1704.

Curry AC (2009) *Biogenic tracers through the Holocene on the Alaskan shelf*. MS Thesis, Old Dominion University, 90 p.

Danielson SL, Weingartner TJ, Hedstrom KS et al. (2014) Coupled wind-forced controls of the Bering-Chukchi shelf circulation and the Bering Strait throughflow: Ekman transport, continental shelf waves, and variations of the Pacific-Arctic sea surface height gradient. *Progress in Oceanography* 125: 40–61.

Darby DA, Bischof J, Cutter G et al. (2001) New record shows pronounced changes in Arctic Ocean circulation and climate. *Eos* 82, No. 49: 601, 607.

Darby DA, Ortiz J, Polyak L et al. (2009) The role of currents and sea ice in both slowly deposited central Arctic and rapidly deposited Chukchi-Alaskan margin sediments. *Global and Planetary Change* 68: 58–72.

Darby DA, Ortiz J, Grosch CE and Lund SP (2012) 1,500-year cycle in the Arctic Oscillation identified in Holocene Arctic sea-ice drift. *Nature Geoscience* 5: 897–900.

de Vernal A, Hillaire-Marcel C and Darby DA (2005) Variability of sea ice cover in the Chukchi Sea (western Arctic Ocean) during the Holocene. *Paleoceanography* 20: PA4018.

de Vernal A, Hillaire-Marcel C, Solignac S et al. (2008) Reconstructing sea ice conditions in the Arctic and sub-Arctic prior to human observations. *Geophysical Monograph* 180, American Geophysical Union, Washington, p. 27–45.

de Vernal A, Hillaire-Marcel C, Rochon A et al. (2013) Dinocyst-based reconstructions of sea ice cover concentration during the Holocene in the Arctic Ocean, the northern North Atlantic Ocean and its adjacent seas. *Quaternary Science Reviews* 79: 111–121.

Dyke AS and Savelle JM (2001) Holocene history of the Bering Sea bowhead whale (Balaena mysticetus) in Its Beaufort Sea summer grounds off southwestern Victoria Island, western Canadian Arctic. *Quaternary Research* 55: 371–379.

Elias S, Short SK and Phillips RL (1992) Paleoecology of late-glacial peats from the Bering land bridge, Chukchi Sea shelf region, northwestern Alaska. *Quaternary Research* 38: 371–378.

Fahl K and Stein R (2012) Modern seasonal variability and deglacial/Holocene change of central Arctic Ocean sea-ice cover: New insights from biomarker proxy records. *Earth and Planetary Science Letters* 351–352: 123–133.

Farmer JR, Cronin TM, de Vernal A et al. (2011) Western Arctic Ocean temperature variability during the last 8000 years. *Geophysical Research Letters* 38: L24602.

Faux JF, Belicka LL, Harvey HR (2011) Organic sources and carbon sequestration in Holocene shelf sediments from the western Arctic Ocean. *Continental Shelf Research* 31: 1169–1179.

Fisher DA, Osterberg E, Dyke A et al. (2008) The Mt. Logan Holocene-late Wisconsinan isotope record: tropical Pacific-Yukon connections. *The Holocene* 18: 667-677.

Funder S, Goosse H, Jepsen H et al. (2011) A 10,000-year record of Arctic Ocean sea-ice variability–View from the beach. *Science* 333: 747–750.

Goňi MA, O'Connor AE, Kuzyk ZZ et al. (2013) Distribution and sources of organic matter in surface marine sediments across the North American Arctic margin. *Journal of Geophysical Research* 118: 4017–4035.

Gonyo AW, Yu Z, Bebout GE (2012) Late Holocene change in climate and atmospheric circulation inferred from geochemical records at Kepler Lake, south-central Alaska. *Journal of Paleolimnology* 48: 55–67.

Haddad RI, Martens CS, Farrington JW (1992) Quantifying early diagenesis of fatty-acids in a rapidly accumulating coastal marine sediment. *Organic Geochemistry* 19: 205– 216.

Harvey HR, Fallon RD, Patton JS (1986) The effect of organic matter and oxygen on the degradation of bacterial membranes lipids in marine sediments. *Geochim. Cosmochim. Acta* 50: 795– 804.

Hetzinger S, Halfar J, Mecking JV et al. (2012) Marine proxy evidence linking decadal North Pacific and Atlantic climate. *Climate Dynamics* 39: 1447–1455.

Hopmans EC, Schouten S, Pancost RD et al. (2000) Analysis of intact tetraether lipids in archaeal cell material and sediments by high performance liquid chromatography/atmospheric pressure chemical ionization mass spectrometry. *Rapid Communications in Mass Spectrometry* 14: 585–589.

Hopmans EC, Weijers JWH, Schefuss E et al. (2004) A novel proxy for terrestrial organic matter in sediments based on branched and isoprenoid tetraether lipids. *Earth and Planetary Science Letters* 24: 107–116.

Huguet C, Hopmans EC, Febo-Ayala W et al. (2006) An improved method to determine the absolute abundance of glycerol dibiphytanyl glycerol tetraether lipids. *Organic Geochemistry* 37: 1036–1041.

Kaufman D, Ager T, Anderson N (2004) Holocene thermal maximum in the western Arctic (0° to 180°W). *Quaternary Science Reviews* 23: 529–560.

Keigwin LD, Donelly JP, Cook MS et al. (2006) Rapid sea-level rise and Holocene climate in the Chukchi Sea. *Geology* 34: 861–864.

Lisé-Pronovost A, St-Onge G, Brachfeld S et al. (2009) Paleomagnetic constraints on the Holocene stratigraphy of the Arctic Alaskan margin. *Global and Planetary Change* 68: 85–99.

MacDonald GM and Case RA (2005) Variations in the Pacific Decadal Oscillation over the past millennium. *Geophyica Research Letters* 32: doi:10.1029/2005GL022478.

Masse G, Rowland SJ, Sicre M-A et al. (2008) Abrupt climate changes for Iceland during the last millennium: Evidence from high resolution sea ice reconstructions. *Earth and Planetary Science Letters* 269: 565–569.

McKay JL, de Vernal A, Hillaire-Marcel C et al. (2008) Holocene fluctuations in Arctic sea-ice cover: dinocyst-based reconstructions for the eastern Chukchi Sea. *Canadian Journal of Earth Sciences* 45: 1377–1397.

McNeely R, Dyke AS and Southon JR (2006) Canadian marine reservoir ages, preliminary data assessment. *Open File Report-Geological Survey of Canada* 5049, 3.

Miller GH, Brigham-Grette J, Alley RB et al. (2010) Arctic amplification: can the past constrain the future? *Quaternary Science Reviews* 29: 1779–1790.

Müller J, Massé G, Stein R, Belt ST (2009) Variability of sea-ice conditions in the Fram Strait over the past 30 000 years. *Nature Geoscience* 2, 772–776

Müller J, Wagner A, Fahl K et al. (2011) Towards quantitative sea ice reconstructions in the northern North Atlantic: a combined biomarker and numerical modelling approach. *Earth and Planetary Science Letters* 306: 137–148.

Müller J, Werner K, Stein R, Fahl K, Moros M, Jansen E (2012) Holocene cooling culminates in sea ice oscillations in Fram Strait. *Quaternary Science Reviews* 47: 1–14.

Nwaodua EC, Ortiz JD and Griffith EM (2014) Diffuse spectral reflectance of surficial sediments indicates sedimentary environments on the shelves of the Bering Sea and western Arctic. *Marine Geology* 355: 218–233.

Ortiz JD, Polyak L, Grebmeier J et al. (2009) Provenance of Holocene sediment on the Chukchi-Alaskan margin based on combined diffuse spectral reflectance and quantitative X-Ray Diffraction analysis. *Global and Planetary Change* 68: 73–84.

Ortiz JD, Nof D, Polyak L et al. (2012) The late Quaternary flow through the Bering Strait has been forced by the Southern Ocean winds. *Journal of Physical Oceanography* 42: 2014–2029.

Park YH, Yamamoto M, Nam S-I et al. (2014) Distribution, source and transportation of glycerol dialkyl glycerol tetraethers in surface sediments from the western Arctic Ocean and the northern Bering Sea. *Marine Chemistry* 165: 10–24.

Pirtle-Levy R, Grebmeier JM, Cooper LW, Larsen IL (2009) Chlorophyll a in Arctic sediments implies long persistence of algal pigments. *Deep-Sea Research II* 56: 1326–1338.

Polyak L, Alley RB, Andrews JT et al. (2010) History of sea ice in the Arctic. *Quaternary Science Reviews* 29: 1757–1778.

Polyak L, Bischof J, Ortiz JD et al. (2009) Late Quaternary stratigraphy and sedimentation patterns in the western Arctic Ocean. *Global and Planetary Change* 68: 5–17.

Porter SEA (2013) *Assessing whether climate variability in the Pacific Basin influences the climate over the North Atlantic and Greenland and modulates sea ice extent*. PhD Thesis, Ohio State University: 222 p.

Reimer PJ, Bard E, Bayliss A et al. (2013) Intcal13 and Marine13 radiocarbon age calibration curves 0–50,000 years cal BP. *Radiocarbon* 55: 1869–1887.

Rontani J-F, Zabeti N, Wakeham SG (2009) The fate of marine lipids: Biotic vs. abiotic degradation of particulate sterols and alkenones in the Northwestern Mediterranean Sea. *Marine Chemistry* 113: 9–18.

Schouten S, Huguet C, Hopmans EC et al. (2007) Analytical methodology for TEX_{86} paleothermometry by high performance liquid chromatography/atmospheric pressure chemical ionization-mass spectrometry. *Analytical Chemistry* 79: 2940–2944.

Shimada K, Kamoshida T, Itoh M et al. (2006) Pacific Ocean inflow: Influence on catastrophic reduction of sea ice cover in the Arctic Ocean. *Geophysical Research Letters* 33: L08605.

Spall MA (2007) Circulation and water mass transformation in a model of the Chukchi Sea. *Journal of Geophysical Research* 112, C05025.

Stoynova V, Shanahan TM, Hughen KA and de Vernal A (2013) Insights into Circum-Arctic sea ice variability from molecular geochemistry. *Quaternary Science Reviews* 79: 63–73.

Stranne C, Jakobsson M and Björk G (2014) Arctic Ocean perennial sea ice breakdown during the Early Holocene Insolation Maximum. *Quaternary Science Reviews* 92: 123–132.

Stroeve JC, Serreze MC, Holland MM et al. (2011) The Arctic's rapidly shrinking sea ice cover: a research synthesis. *Climatic Change*: DOI 10.1007/s10584-011-0101-1.

Vare LL, Masse G, Gregory TR (2009) Sea ice variations in the central Canadian Arctic Archipelago during the Holocene. *Quaternary Science Reviews* 28: 1354–1366.

Weckström K, Massé G, Collins LG et al. (2013) Evaluation of the sea ice proxy IP_{25} against observational and diatom proxy data in the SW Labrador Sea. *Quaternary Science Reviews* 79: 53–62.

Weingartner T, Aagaard K, Woodgate R et al. (2005) Circulation on the north central Chukchi Sea shelf. *Deep-Sea Research II* 52: 3150–3174.

Winsor P and Chapman DC (2004) Pathways of Pacific water across the Chukchi Sea: A numerical model study. *Journal of Geophysical Research* 109: C03002.

Woodgate RA, Weingartner T and Lindsay R (2010) The 2007 Bering Strait oceanic heat flux and anomalous Arctic sea-ice retreat. *Geophysical Research Letters* 37: L01602.

Xiao X, Fahl K, Müller J and Stein R (2015a) Sea-ice distribution in the modern Arctic Ocean: Biomarker records from trans-Arctic Ocean surface sediments. *Geochimica et Cosmochimica Acta* 155, 16–29.

Xiao X, Stein R and Fahl K (2015b) MIS 3 to MIS 1 temporal and LGM spatial variability in Arctic Ocean sea ice cover: reconstruction from biomarkers. *Paleoceanography* 30, doi:10.1002/ 2015PA002814.

Zhang X, Sorteberg A, Zhang J et al. (2008) Recent radical shifts of atmospheric circulations and rapid changes in Arctic climate system. *Geophysical Research Letters* 35: L22701.

Figure captions

Figure 1. Index map of the western Arctic Ocean and the study area (inset). Shown are cores under study (red circles) and related cores: purple – CAA IP_{25} records (Belt et al., 2010), orange circles/squares in inset – long/box-cores with dinocyst-based reconstructions, grey – other cores from proxy studies mentioned in the paper. Yellow and orange lines show September (yearly minimum) ice extent (15% concentration): late 20th century mean and 2012 historical minimum. Pink field south of the mean ice extent encloses maximal concentrations of IP_{25} measured in surface sediments (Stoynova et al., 2013). Arrows in inset show Bering Strait Inflow branches (blue) and Beaufort Gyre (violet). BC – Barrow Canyon, BS – Bering Strait, CAA – Canadian Arctic Archipelago.

Figure 2. Distribution of IP_{25}, sterols, and total organic carbon in cores 5TC/JPC and 8 MC/TC/JPC vs. composite core depth. OC data are from McKay et al. (2008) and Curry (2009) for 5JPC and 8JPC, respectively. IP_{25} and sterol data presented in μg/cm^3 sediment. ^{14}C ages (cal ka BP) are shown at the core depth axes. Grey vertical line – bottom of marine unit. Sampling levels in JPCs are shown by dots; no symbols are used for more densely sampled MC/TCs and for OC data. Scale bars for some proxies may slightly differ between the cores for illustrative purposes.

Figure 3. Distribution of IP_{25} and related proxies in cores 5TC/JPC and 8 MC/TC/JPC vs. age: IP_{25}, PIP_{25} indices, isoprenoid GDGT concentrations, and linear sedimentation rates (LSR). Samples are indicated by dots in JPCs and by crosses in 8 MC/TC; no symbols are used for

densely sampled 5 TC. Yellow field on the left highlights subsurface interval with elevated sterol concentrations. PIP_{25} indices are calculated using separate balance factors for <0.4-0.5-ka and older intervals. Also shown is a dinocyst-based reconstruction of sea-ice duration (months/year) for 5TC/JPC (Farmer et al., 2011; ages recalibrated). Grey vertical line – bottom of marine unit. Dashed lines near the JPC8 bottom – alternative age model due to ^{14}C inversion.

Figure 4. Distribution of brassicasterol vs. terrestrial sterols, dinosterol, and IP_{25} in cores under study. All data presented in μg/cm^3 sediment. Different symbols indicate two distinctly different patterns: in the subsurface interval (younger than ~ 0.4-0.5 ka) and in the rest of the record.

Figure 5. Comparison of the distribution of brassicasterol vs. IP_{25} in cores under study and surface sediments of the Chukchi Sea and North Pacific (data from Stoynova et al., 2013). All data presented in μg/g sediment for compatibility. Grey circles – 5JPC, plus signs – 8JPC; orange and blue dots – surface sediment samples from the Chukchi Sea and North Pacific, respectively.

Figure 6. Conceptual scheme of circulation and sea-ice extent at the Chukchi-Alaskan margin during the early and middle Holocene (roughly, 7-10 and 4-7 ka, respectively) in comparison with recent conditions (Fig. 1 for more detail). Arrows show Bering Strait Inflow; thicker arrows indicate higher current strength. Yellow line indicates inferred patterns of Holocene summer ice margin (a, b) and observed late 20th century ice extent (c). Red dots show location of cores under study.

Figure7. Comparison of IP_{25} data from the Chukchi-Alaskan margin (this study) and the Canadian Arctic Archipelago (CAA) straits (Figure 1 for site location; Vare et al., 2009; Belt et al., 2010). The CAA IP_{25} datasets are shown in relative abundance because of vastly different concentrations, with an offset for illustrative purposes. Grey bar marks the period of increased Bering Strait Inflow inferred from a sedimentary proxy record (Ortiz et al., 2009, 2012).

Figure8. IP_{25} and sterol data for the last millennium (this study), compared to IP_{25} records from the CAA (Belt et al., 2010), dinocyst-based sea-ice proxy curves (5TC: Farmer et al., 2011; B5: de Vernal et al., 2008), and Arctic-wide reconstruction of sea-ice extent (Kinnard et al., 2011). Red horizontal bars show the range of ^{210}Pb data for 5TC and B5 (McKay et al., 2008; de Vernal et al., 2008). Vertical pink and light blue fields indicate early and late Little Ice Age in the Arctic-Pacific region. IP_{25} and sterol data are presented in µg/cm^3 sediment. Brassicasterol and terrestrial sterol profiles are quadratically detrended. Scale bars for some proxies may slightly differ between the cores for illustrative purposes.

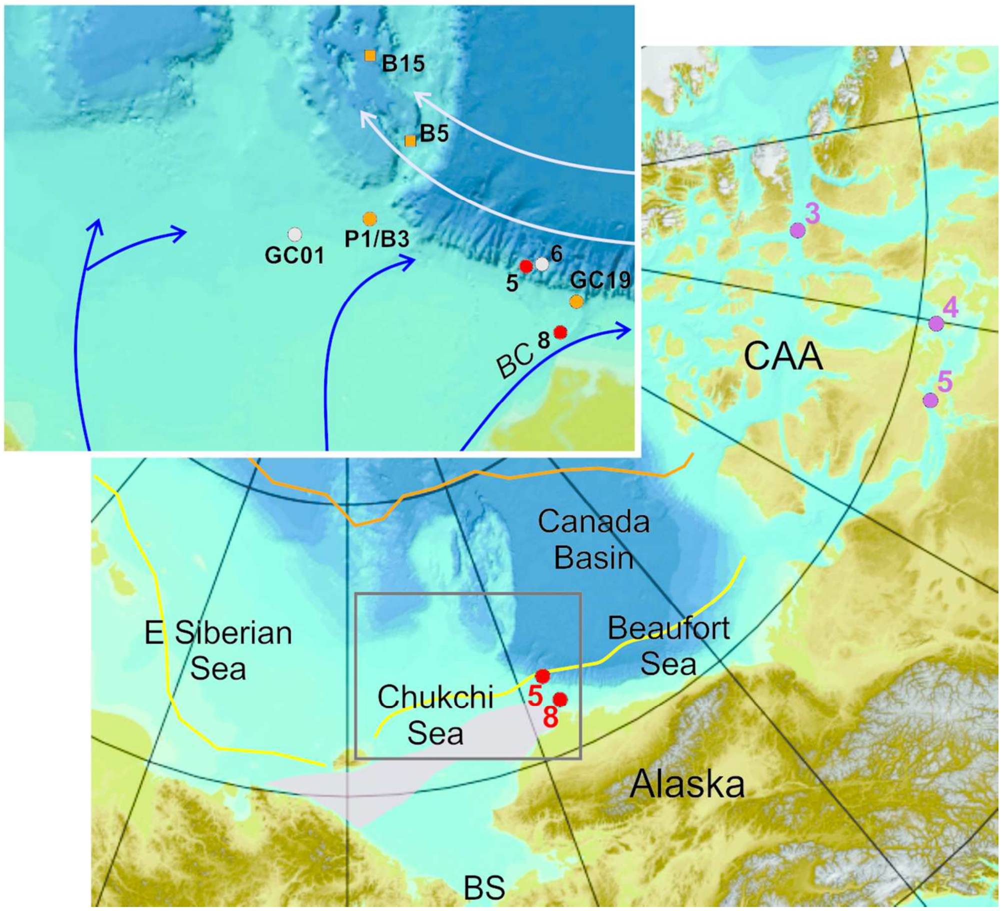

Figure 1. Index map of the western Arctic Ocean and the study area (inset). Shown are cores under study (red circles) and related cores: purple – CAA IP25 records (Belt et al., 2010), orange circles/squares in inset – long/box-cores with dinocyst-based reconstructions, grey – other cores from proxy studies mentioned in the paper. Yellow and orange lines show September (yearly minimum) ice extent (15% concentration): late 20th century mean and 2012 historical minimum. Pink field south of the mean ice extent encloses maximal concentrations of IP25 measured in surface sediments (Stoynova et al., 2013). Arrows in inset show Bering Strait Inflow branches (blue) and Beaufort Gyre (violet). BC – Barrow Canyon, BS – Bering Strait, CAA – Canadian Arctic Archipelago.
109x99mm (300 x 300 DPI)

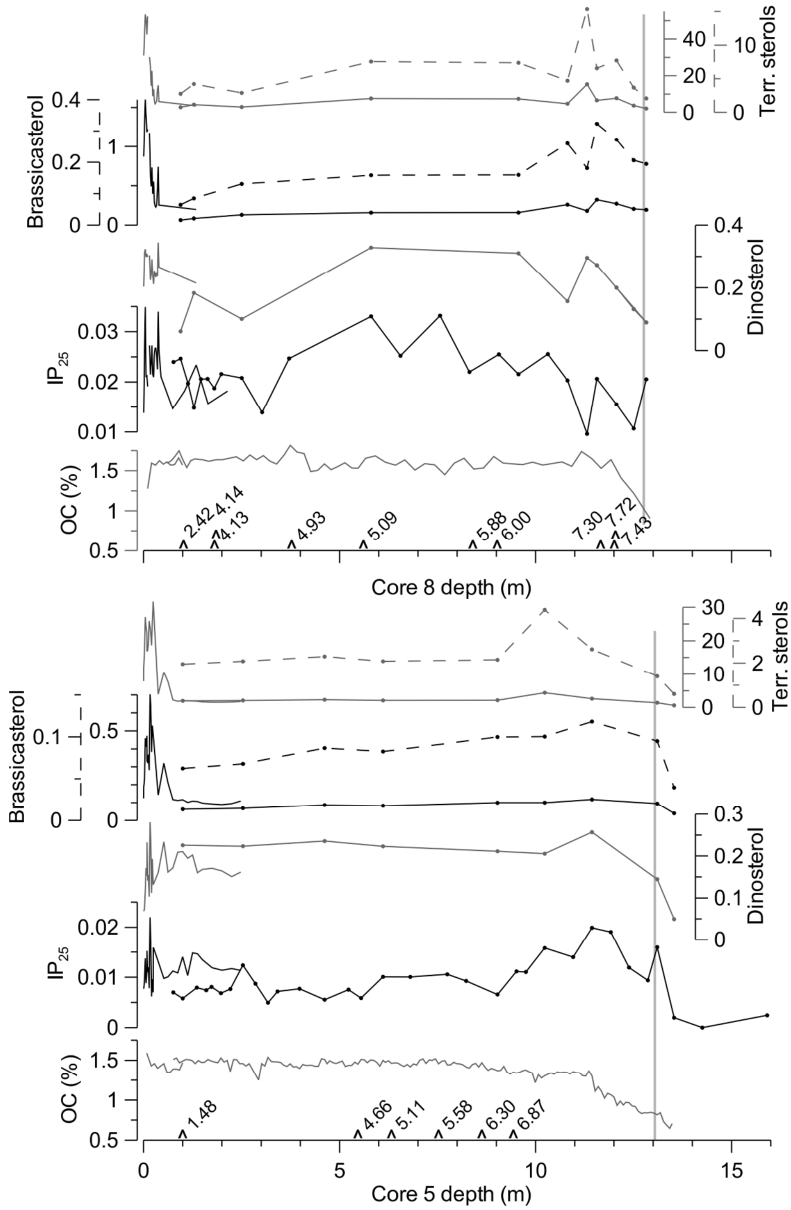

Figure 2. Distribution of IP25, sterols, and total organic carbon in cores 5TC/JPC and 8 MC/TC/JPC vs. composite core depth. OC data are from McKay et al. (2008) and Curry (2009) for 5JPC and 8JPC, respectively. IP25 and sterol data presented in μg/cm3 sediment. 14C ages (cal ka BP) are shown at the core depth axes. Grey vertical line – bottom of marine unit. Sampling levels in JPCs are shown by dots; no symbols are used for more densely sampled MC/TCs and for OC data. Scale bars for some proxies may slightly differ between the cores for illustrative purposes.
157x242mm (300 x 300 DPI)

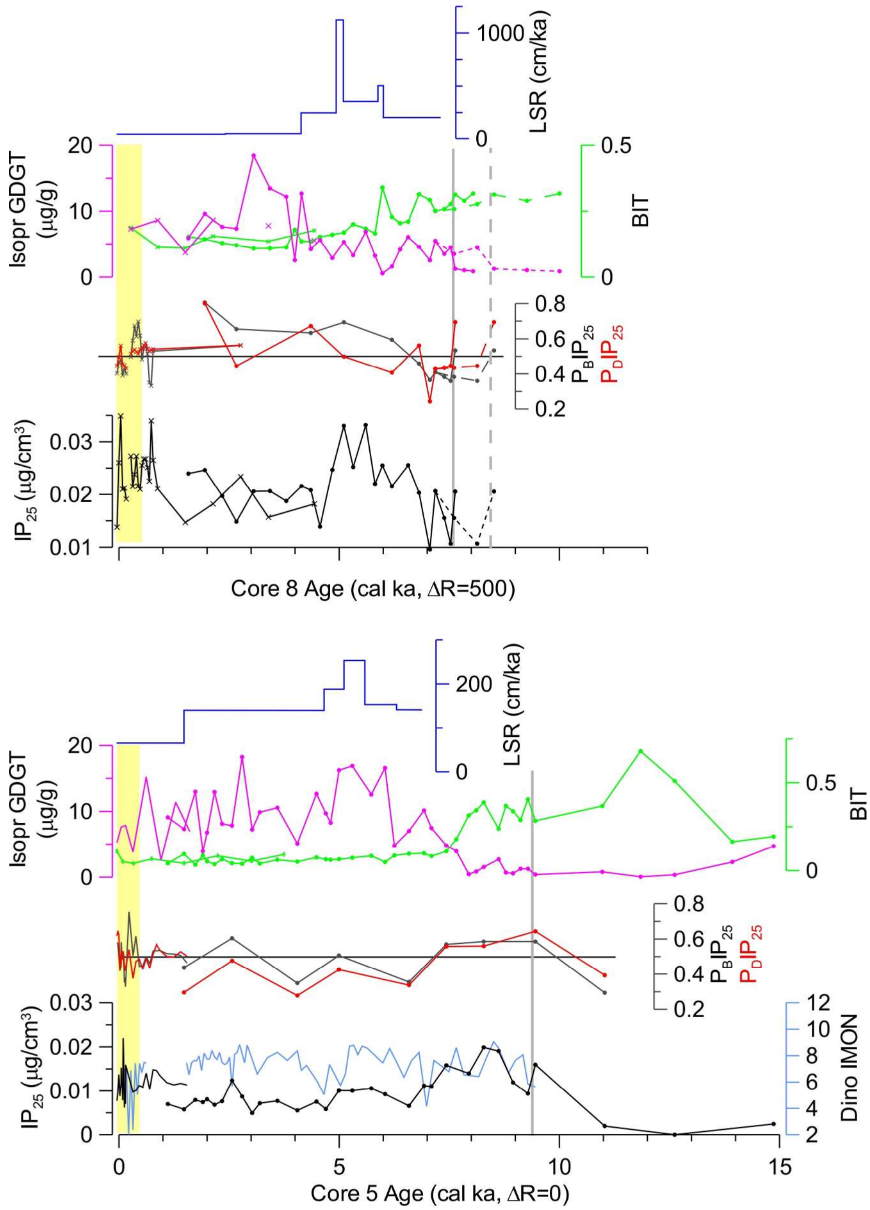

Figure 3. Distribution of IP25 and related proxies in cores 5TC/JPC and 8 MC/TC/JPC vs. age: IP25, PIP25 indices, isoprenoid GDGT concentrations, and linear sedimentation rates (LSR). Samples are indicated by dots in JPCs and by crosses in 8 MC/TC; no symbols are used for densely sampled 5 TC. Yellow field on the left highlights subsurface interval with elevated sterol concentrations. PIP25 indices are calculated using separate balance factors for <0.4-0.5-ka and older intervals. Also shown is a dinocyst-based reconstruction of sea-ice duration (months/year) for 5TC/JPC (Farmer et al., 2011; ages recalibrated). Grey vertical line – bottom of marine unit. Dashed lines near the JPC8 bottom – alternative age model due to 14C inversion.
164x230mm (300 x 300 DPI)

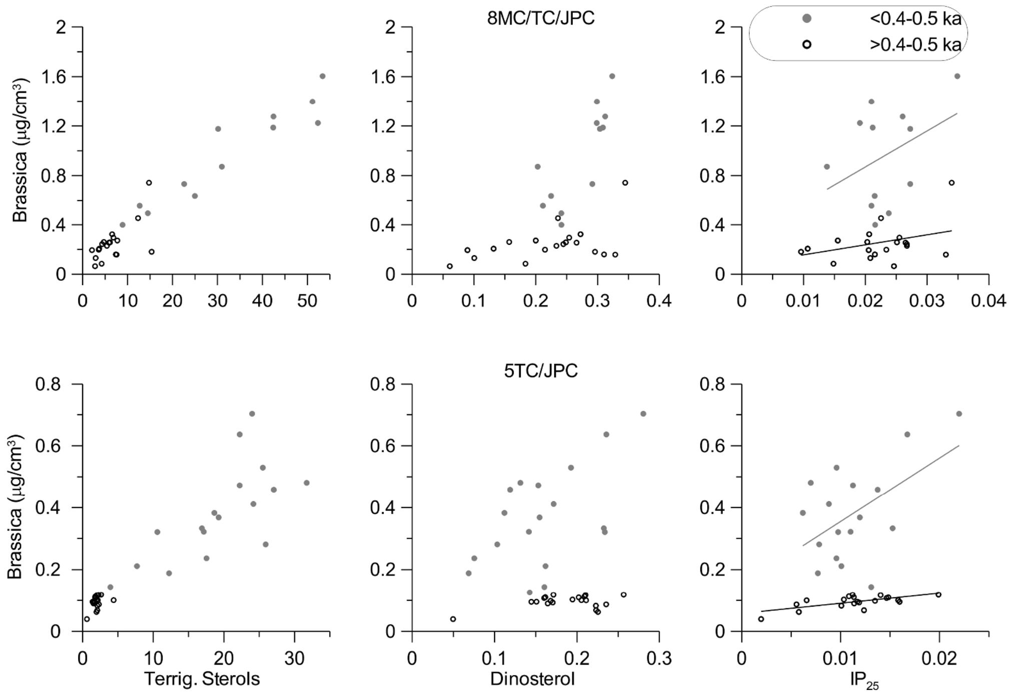

Figure 4. Distribution of brassicasterol vs. terrestrial sterols, dinosterol, and IP25 in cores under study. All data presented in μg/cm3 sediment. Different symbols indicate two distinctly different patterns: in the subsurface interval (younger than ~ 0.4-0.5 ka) and in the rest of the record.
230x157mm (300 x 300 DPI)

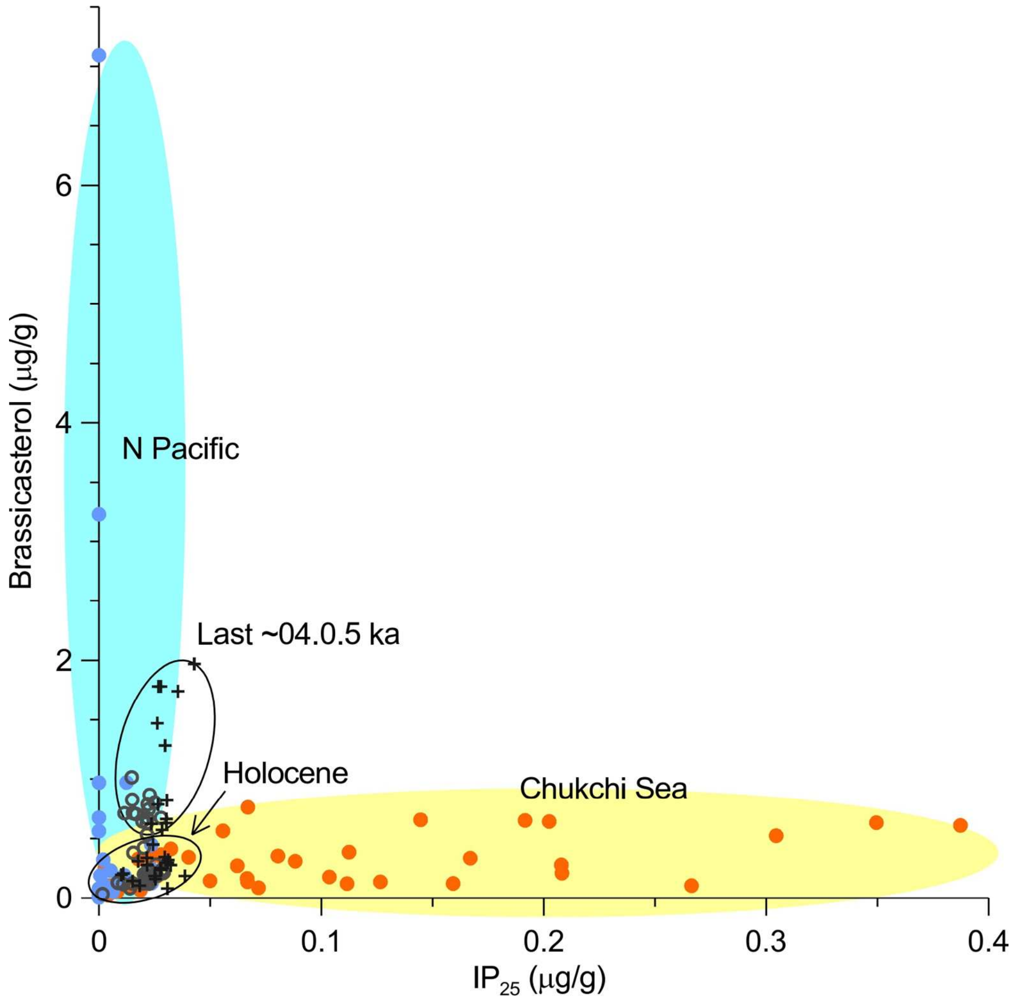

Figure 5. Comparison of the distribution of brassicasterol vs. IP25 in cores under study and surface sediments of the Chukchi Sea and North Pacific (data from Stoynova et al., 2013). All data presented in μg/g sediment for compatibility. Grey circles – 5JPC, plus signs – 8JPC; orange and blue dots – surface sediment samples from the Chukchi Sea and North Pacific, respectively.
142x141mm (300 x 300 DPI)

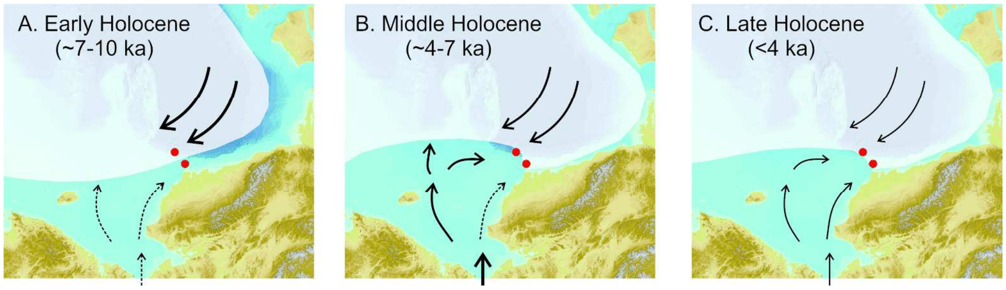

Figure 6. Conceptual scheme of circulation and sea-ice extent at the Chukchi-Alaskan margin during the early and middle Holocene (roughly, 7-10 and 4-7 ka, respectively) in comparison with recent conditions (Fig. 1 for more detail). Arrows show Bering Strait Inflow; thicker arrows indicate higher current strength. Yellow line indicates inferred patterns of Holocene summer ice margin (a, b) and observed late 20th century ice extent (c). Red dots show location of cores under study.
228x64mm (300 x 300 DPI)

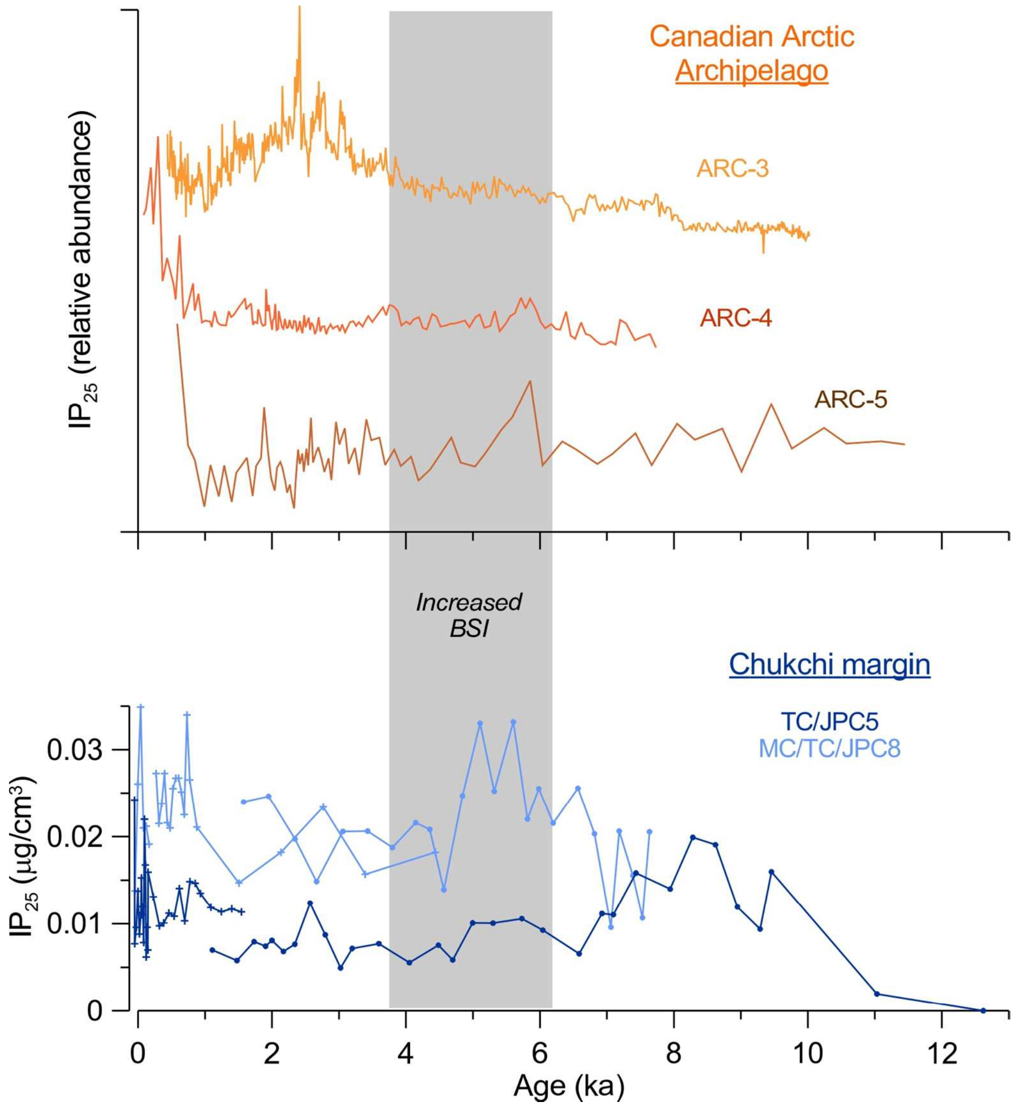

Figure7. Comparison of IP25 data from the Chukchi-Alaskan margin (this study) and the Canadian Arctic Archipelago (CAA) straits (Figure 1 for site location; Vare et al., 2009; Belt et al., 2010). The CAA IP25 datasets are shown in relative abundance because of vastly different concentrations, with an offset for illustrative purposes. Grey bar marks the period of increased Bering Strait Inflow inferred from a sedimentary proxy record (Ortiz et al., 2009, 2012).
145x159mm (300 x 300 DPI)

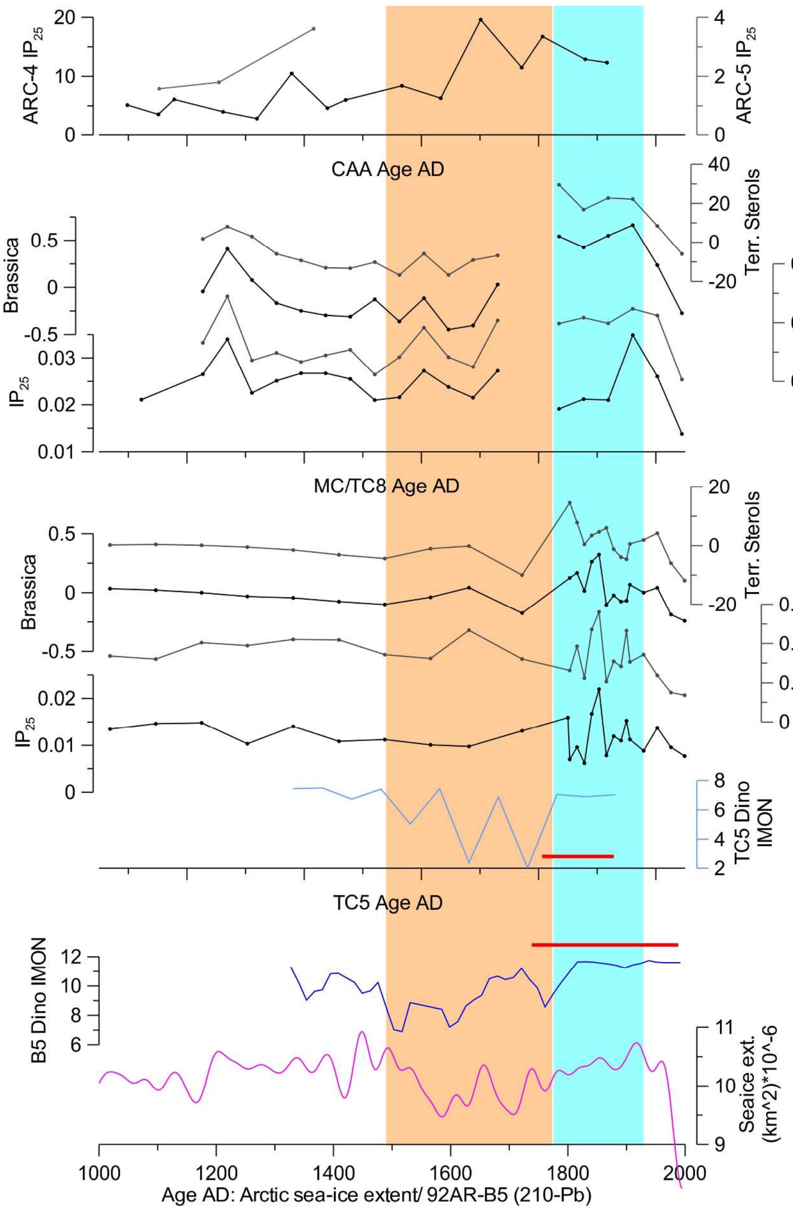

Figure8. IP25 and sterol data for the last millennium (this study), compared to IP25 records from the CAA (Belt et al., 2010), dinocyst-based sea-ice proxy curves (5TC: Farmer et al., 2011; B5: de Vernal et al., 2008), and Arctic-wide reconstruction of sea-ice extent (Kinnard et al., 2011). Red horizontal bars show the range of 210Pb data for 5TC and B5 (McKay et al., 2008; de Vernal et al., 2008). Vertical pink and light blue fields indicate early and late Little Ice Age in the Arctic-Pacific region. IP25 and sterol data are presented in μg/cm3 sediment. Brassicasterol and terrestrial sterol profiles are quadratically detrended. Scale bars for some proxies may slightly differ between the cores for illustrative purposes.
180x259mm (300 x 300 DPI)

Supplemental information for "Holocene sea-ice conditions and circulation at the Chukchi-Alaskan margin, Arctic Ocean, inferred from biomarker proxies"

Leonid Polyak[1], Simon T. Belt[2], Patricia Cabedo-Sanz[2], Masanobu Yamamoto[3], Yu-Hyeon Park[3,4]

[1] Byrd Polar and Climate Research Center, Ohio State University, Columbus, OH, USA

[2] Biogeochemistry Research Centre, University of Plymouth, Plymouth, UK

[3] Environmental and Earth Science, Hokkaido University, Sapporo, Japan

[4] Pusan National University, Pusan, Korea

Corresponding author:

Leonid Polyak, Byrd Polar and Climate Research Center, Ohio State University, Columbus, OH 43210, USA. Email: polyak.1@osu.edu

Supplement 1. Age constraints for sediment cores HLY0501-5 and 8 used in this study.

Station	Core	Core depth (cm)	^{14}C Age	Cal BP (Calib7)	Type of age tie point	Source
HLY0501-5	JPC	25	1930	1477	^{14}C age	Darby et al., 2009
HLY0501-5		472	4465	4655	^{14}C age	Darby et al., 2009
HLY0501-5		557.5	4820	5109	^{14}C age	Darby et al., 2009
HLY0501-5		677.5	5220	5583	^{14}C age	Darby et al., 2009
HLY0501-5		788	5885	6303	^{14}C age	Darby et al., 2009
HLY0501-5		868.5	6395	6870	^{14}C age	Darby et al., 2009
HLY0501-5		1240		9487	extrapolation to unit bottom	
HLY0501-5		1305		12000	regional context	Polyak et al., 2009
HLY0501-5		1526		15000	regional context	Polyak et al., 2009
HLY0501-8	TC	185	4,591	4137	^{14}C age	Darby et al., 2009
HLY0501-8	JPC	51	3,216	2416	^{14}C age	Darby et al., 2009
HLY0501-8		130	4,590	4135	^{14}C age	Darby et al., 2009
HLY0501-8		327	5,210	4931	^{14}C age	Darby et al., 2009
HLY0501-8		510	5,309	5094	^{14}C age	Darby et al., 2009
HLY0501-8		789	5,995	5880	^{14}C age	Darby et al., 2009
HLY0501-8		851	6,110	6003	^{14}C age	Darby et al., 2009
HLY0501-8		1115	7,275	7304	^{14}C age	Darby et al., 2009
HLY0501-8		1150	7,760	7722	^{14}C age	Darby et al., 2009
HLY0501-8		1153	7,415	7428	^{14}C age	Darby et al., 2009

Radiocarbon ages were calibrated using CALIB 7.0 with ΔR assumed as 0 and 500 for HLY0501-5 and HLY0501-8, respectively. See main text for more detail.

Supplement 2. IP_{25} and sterol data for cores HLY0501-5 and 8.

Station	Core	Sample center depth	Cal age (ka BP)	IP_{25} (µg/cm^3)	Brassica-sterol (µg/cm3)	Dinosterol (µg/cm3)	Terrigenous sterols (µg/cm3)
HLY0501-5	TC	0.5	-0.049	0.007699	0.188279	0.06852	12.23648
HLY0501-5	TC	2.5	-0.026	0.009576	0.236325	0.075365	17.540558
HLY0501-5	TC	4.5	-0.003	0.013746	0.458306	0.118893	27.066396
HLY0501-5	TC	6.5	0.021	0.008818	0.41122	0.171684	24.179891
HLY0501-5	TC	8.5	0.044	0.011247	0.472235	0.153068	22.234378
HLY0501-5	TC	9	0.050	0.01526	0.333003	0.232585	16.885332
HLY0501-5	TC	10.5	0.059	0.011007	0.321691	0.141645	17.148304
HLY0501-5	TC	12.5	0.072	0.011946	0.367989	0.154587	19.256986
HLY0501-5	TC	14.5	0.084	0.007831	0.281074	0.103233	25.916338
HLY0501-5	TC	16.5	0.097	0.021987	0.702991	0.280529	23.993149
HLY0501-5	TC	18.5	0.109	0.016747	0.636437	0.235668	22.238188
HLY0501-5	TC	20.5	0.122	0.006178	0.38256	0.111924	18.649615
HLY0501-5	TC	22.5	0.134	0.009591	0.52945	0.192755	25.515621
HLY0501-5	TC	24.5	0.147	0.006982	0.480703	0.131306	31.72491
HLY0501-5	TC	25	0.150	0.01592			
HLY0501-5	TC	37.5	0.228	0.013098	0.143423	0.160437	3.9224915
HLY0501-5	TC	52	0.319	0.00975	0.320793	0.233815	10.577303
HLY0501-5	TC	62.5	0.384	0.010078	0.211069	0.161807	7.6932024
HLY0501-5	TC	75	0.463	0.011215	0.117877	0.171462	2.2597986
HLY0501-5	TC	87.5	0.541	0.010843	0.112848	0.209233	1.8252641
HLY0501-5	TC	100	0.619	0.014042	0.116667	0.210376	2.0502299
HLY0501-5	TC	112.5	0.697	0.010329	0.102373	0.194562	1.9853376
HLY0501-5	TC	125	0.775	0.014832	0.109335	0.202146	1.894453
HLY0501-5	TC	137.5	0.853	0.014641	0.107211	0.160189	1.8261713
HLY0501-5	TC	150	0.931	0.01348	0.09808	0.168063	1.6317405
HLY0501-5	TC	175	1.088	0.011875	0.09282	0.170553	1.5543043
HLY0501-5	TC	200	1.244	0.011364	0.089684	0.164487	1.5398369
HLY0501-5	TC	225	1.400	0.011697	0.095202	0.150803	1.6309574
HLY0501-5	TC	248	1.544	0.01134	0.10997	0.161555	1.7553619
HLY0501-5	JPC	1	1.306	0.006976			
HLY0501-5	JPC	25	1.477	0.005778	0.062368	0.225509	1.9543
HLY0501-5	JPC	61	1.733	0.007934			
HLY0501-5	JPC	85	1.904	0.007414			
HLY0501-5	JPC	98.5	2.000	0.008079			
HLY0501-5	JPC	122.5	2.170	0.006815			
HLY0501-5	JPC	146.5	2.341	0.007642			
HLY0501-5	JPC	178.5	2.568	0.012369	0.067848	0.223263	2.0784604
HLY0501-5	JPC	210.5	2.796	0.008716			
HLY0501-5	JPC	242.5	3.023	0.004937			
HLY0501-5	JPC	267	3.198	0.007163			
HLY0501-5	JPC	323	3.596	0.007705			
HLY0501-5	JPC	387	4.051	0.005535	0.08665	0.235418	2.2947813
HLY0501-5	JPC	448	4.484	0.007531			
HLY0501-5	JPC	480	4.697	0.005847			
HLY0501-5	JPC	536	4.995	0.010076	0.082541	0.222928	2.0830645
HLY0501-5	JPC	605.5	5.299	0.010053			
HLY0501-5	JPC	700	5.730	0.010568			

Station	Core	Sample center depth	Cal age (ka BP)	IP_{25} (µg/cm^3)	Brassica-sterol (µg/cm3)	Dinosterol (µg/cm3)	Terrigenous Sterols (µg/cm3)
HLY0501-5	JPC	748	6.042	0.009252			
HLY0501-5	JPC	828	6.585	0.006561	0.099808	0.211102	2.1500828
HLY0501-5	JPC	876.5	6.926	0.011159			
HLY0501-5	JPC	900.5	7.095	0.01103			
HLY0501-5	JPC	948.5	7.433	0.01582	0.100312	0.205391	4.3823689
HLY0501-5	JPC	1021	7.944	0.013993			
HLY0501-5	JPC	1069	8.282	0.019902	0.118214	0.256681	2.6150212
HLY0501-5	JPC	1117	8.620	0.019054			
HLY0501-5	JPC	1163.5	8.948	0.011921			
HLY0501-5	JPC	1211.5	9.286	0.009384			
HLY0501-5	JPC	1235.5	9.455	0.015962	0.094899	0.144625	1.4042965
HLY0501-5	JPC	1278.5	11.030	0.001963	0.039512	0.049599	0.6074161
HLY0501-5	JPC	1350.5	12.618	0			
HLY0501-5	JPC	1516	14.864	0.002439			
HLY0501-8	MC	0.5	-0.045	0.013789	0.871922	0.203062	30.978487
HLY0501-8	MC	2.5	-0.003	0.026038	1.275847	0.312249	42.464423
HLY0501-8	MC	4.5	0.039	0.034889	1.603823	0.323684	53.391038
HLY0501-8	MC	6.5	0.081	0.020989	1.397614	0.298995	51.149718
HLY0501-8	MC	8.5	0.123	0.02119	1.186479	0.308625	42.407771
HLY0501-8	MC	10.5	0.165	0.019121	1.223574	0.298633	52.351094
HLY0501-8	TC	0.5	0.270	0.027268	1.175859	0.303827	30.149569
HLY0501-8	TC	2.5	0.312	0.021509	0.636337	0.224713	24.96717
HLY0501-8	TC	4.5	0.354	0.023795	0.492997	0.241383	14.508526
HLY0501-8	TC	6.5	0.396	0.02727	0.732594	0.291511	22.590786
HLY0501-8	TC	8.5	0.438	0.02159	0.399129	0.241453	8.8851625
HLY0501-8	TC	10.5	0.479	0.020987	0.553618	0.211559	12.689041
HLY0501-8	TC	12.5	0.521	0.025514	0.295807	0.254068	6.8400249
HLY0501-8	TC	14.5	0.563	0.026718	0.24309	0.244567	4.3283088
HLY0501-8	TC	16.5	0.605	0.026726	0.229232	0.233367	5.3911914
HLY0501-8	TC	18.5	0.647	0.025114	0.257613	0.248689	6.083661
HLY0501-8	TC	20.5	0.689	0.022536	0.453579	0.235888	12.324573
HLY0501-8	TC	22.5	0.731	0.03398	0.742786	0.34473	14.757235
HLY0501-8	TC	24.5	0.773	0.026506	0.255071	0.266003	5.8676942
HLY0501-8	TC	29.5	0.878	0.021084			
HLY0501-8	TC	59.5	1.507	0.014687			
HLY0501-8	TC	89.5	2.135	0.018207			
HLY0501-8	TC	119.5	2.764	0.0234	0.198148	0.214934	3.5653505
HLY0501-8	TC	149.5	3.393	0.01568			
HLY0501-8	TC	199.5	4.437	0.018195			
HLY0501-8	JPC	10.5	1.576	0.023978			
HLY0501-8	JPC	28.5	1.949	0.024629	0.064632	0.06084	2.7589244
HLY0501-8	JPC	47.5	2.343	0.019714			
HLY0501-8	JPC	62.5	2.666	0.014843	0.084972	0.183274	4.2214515
HLY0501-8	JPC	80.5	3.058	0.020581			
HLY0501-8	JPC	97.5	3.428	0.020621			
HLY0501-8	JPC	114.5	3.798	0.01874			
HLY0501-8	JPC	132.5	4.145	0.021581			
HLY0501-8	JPC	184.5	4.355	0.020812	0.130839	0.100434	2.8907779

Station	Core	Sample center depth (cm)	Cal age (ka BP)	IP_{25} (µg/cm^3)	Brassica-sterol (µg/cm3)	Dinosterol (µg/cm3)	Terrigenous Sterols (µg/cm3)
HLY0501-8	JPC	236.5	4.565	0.013904			
HLY0501-8	JPC	305.5	4.844	0.024681			
HLY0501-8	JPC	514.5	5.107	0.033034	0.1585	0.328597	7.5562627
HLY0501-8	JPC	589.5	5.318	0.025215			
HLY0501-8	JPC	690.5	5.603	0.033184			
HLY0501-8	JPC	765.5	5.814	0.022007			
HLY0501-8	JPC	840.5	5.982	0.025505			
HLY0501-8	JPC	890.5	6.198	0.021548	0.159757	0.310475	7.3749341
HLY0501-8	JPC	965.5	6.567	0.025553			
HLY0501-8	JPC	1015.5	6.814	0.020316	0.260379	0.156992	4.7078924
HLY0501-8	JPC	1065.5	7.060	0.009596	0.181261	0.295871	15.350514
HLY0501-8	JPC	1090.5	7.183	0.020628	0.323257	0.272446	6.5603022
HLY0501-8	JPC	1140.5	7.387	0.015543	0.272364	0.199961	7.7201214
HLY0501-8	JPC	1184.5	7.531	0.010676	0.206253	0.131675	3.6842771
HLY0501-8	JPC	1216.5	7.635	0.020543	0.194695	0.089423	2.0737872
HLY0501-8	JPC	1140.5	7.609	0.015543	0.323257	0.272446	6.5603022
HLY0501-8	JPC	1184.5	8.134	0.010676	0.272364	0.199961	7.7201214
HLY0501-8	JPC	1216.5	8.516	0.020543	0.206253	0.131675	3.6842771
					0.194695	0.089423	2.0737872

Age model is constructed by interpolation between tie points (Suppl. 1) and modern age (2005, year of collection) assumed for the top of HLY0501-5TC and 8MC.

5JPC to TC and 8JPC to TC offests were estimated as 75 and 51 cm, respectively. 8TC to MC offset was estimated as 15 cm.

Alternative age models are shown for the bottom part of 8JPC (three lowermost samples) due to an age inversion.

Age model for 5TC is based on the extrapolation of sedimentation rates estimated from ^{210}Pb data in the top 15 cm (McKay et al., 2008).

Supplement 3. Isoprenoid GDGT data for cores HLY0501-5 and 8.

Station	Core	Sample center depth (cm)	Cal age (ka BP)	Isoprenoid GDGT (µg/g)
HLY0501-5	TC	0.5	-0.047	5.263
HLY0501-5	TC	9	0.050	7.6478
HLY0501-5	TC	25	0.150	7.8684
HLY0501-5	TC	52	0.319	3.8109
HLY0501-5	TC	100	0.619	15.2172
HLY0501-5	TC	150	0.953	2.5701
HLY0501-5	TC	200	1.288	11.4015
HLY0501-5	TC	248	1.609	6.952709
HLY0501-5	JPC	1	1.109	9.0967
HLY0501-5	JPC	25	1.477	7.3033
HLY0501-5	JPC	61	1.733	12.9878
HLY0501-5	JPC	85	1.904	3.9244
HLY0501-5	JPC	98.5	2.000	6.7827
HLY0501-5	JPC	122.5	2.170	12.9493
HLY0501-5	JPC	146.5	2.341	8.117
HLY0501-5	JPC	178	2.565	7.8463
HLY0501-5	JPC	210.5	2.796	18.238
HLY0501-5	JPC	242.5	3.023	7.2435
HLY0501-5	JPC	267	3.198	9.8737
HLY0501-5	JPC	323	3.596	10.5682
HLY0501-5	JPC	387	4.051	5.1209
HLY0501-5	JPC	448	4.484	12.68
HLY0501-5	JPC	480	4.697	9.6894
HLY0501-5	JPC	500.5	4.806	8.274
HLY0501-5	JPC	536.5	4.997	16.2453
HLY0501-5	JPC	605.5	5.299	16.9074
HLY0501-5	JPC	700	5.730	12.571
HLY0501-5	JPC	748	6.042	16.5883
HLY0501-5	JPC	780.5	6.254	4.7828
HLY0501-5	JPC	828	6.585	7.0139
HLY0501-5	JPC	876.5	6.926	10.1534
HLY0501-5	JPC	900.5	7.095	7.4662
HLY0501-5	JPC	948.5	7.433	4.7995
HLY0501-5	JPC	980.5	7.659	3.9545
HLY0501-5	JPC	1021	7.944	0.4549
HLY0501-5	JPC	1045	8.113	0.8556
HLY0501-5	JPC	1069	8.282	1.5306
HLY0501-5	JPC	1117	8.620	2.7178
HLY0501-5	JPC	1140.5	8.786	0.6985
HLY0501-5	JPC	1163.5	8.948	0.5824
HLY0501-5	JPC	1187.5	9.117	1.2696
HLY0501-5	JPC	1211.5	9.286	1.2699
HLY0501-5	JPC	1235.5	9.455	0.4045
HLY0501-5	JPC	1278.5	10.975	0.7962
HLY0501-5	JPC	1301	11.845	0.0609
HLY0501-5	JPC	1350.5	12.618	0.3515
HLY0501-5	JPC	1447	13.928	2.3005
HLY0501-5	JPC	1516	14.864	4.7049

Station	Core	Sample center depth (cm)	Cal age (ka BP)	Isoprenoid GDGT (µg/g)
HLY0501-8	TC	0.5	0.270	7.2882
HLY0501-8	TC	29.5	0.878	8.610142
HLY0501-8	TC	59.5	1.507	3.724501
HLY0501-8	TC	89.5	2.135	8.639842
HLY0501-8	TC	149.5	3.393	7.785916
HLY0501-8	TC	199.5	4.438	5.515085
HLY0501-8	JPC	10.5	1.576	5.8992
HLY0501-8	JPC	28.5	1.949	9.5994
HLY0501-8	JPC	47.5	2.343	7.6111
HLY0501-8	JPC	62.5	2.666	7.3341
HLY0501-8	JPC	80.5	3.058	18.436
HLY0501-8	JPC	97.5	3.428	13.4463
HLY0501-8	JPC	114.5	3.798	12.1931
HLY0501-8	JPC	123.5	3.994	2.5473
HLY0501-8	JPC	132.5	4.145	12.6769
HLY0501-8	JPC	184.5	4.355	4.2261
HLY0501-8	JPC	236.5	4.565	5.6193
HLY0501-8	JPC	305.5	4.844	2.8884
HLY0501-8	JPC	514.5	5.107	5.3138
HLY0501-8	JPC	589.5	5.318	3.3047
HLY0501-8	JPC	690.5	5.603	6.8812
HLY0501-8	JPC	765.5	5.814	3.2245
HLY0501-8	JPC	840.5	5.982	0.5612
HLY0501-8	JPC	890.5	6.198	1.608
HLY0501-8	JPC	928	6.382	4.1639
HLY0501-8	JPC	965.5	6.567	6.0575
HLY0501-8	JPC	1015.5	6.814	4.5665
HLY0501-8	JPC	1065.5	7.060	2.532
HLY0501-8	JPC	1090.5	7.183	5.463
HLY0501-8	JPC	1140.5	7.387	3.5019
HLY0501-8	JPC	1184.5	7.531	4.4858
HLY0501-8	JPC	1216.5	7.635	1.2512
HLY0501-8	JPC	1279	7.839	1.0323
HLY0501-8	JPC	1341	8.041	0.87
HLY0501-8	JPC	1140.5	7.609	3.5019
HLY0501-8	JPC	1184.5	8.134	4.4858
HLY0501-8	JPC	1216.5	8.516	1.2512
HLY0501-8	JPC	1279	9.263	1.0323
HLY0501-8	JPC	1341	10.003	0.87

Age model is constructed by interpolation between tie points (Suppl. 1) and modern age (2005, year of collection) assumed for the top of HLY0501-5TC and 8MC.

5JPC to TC and 8JPC to TC offests were estimated as 75 and 51 cm, respectively. 8TC to MC offset was estimated as 15 cm.

Alternative age models are shown for the bottom part of 8JPC (five lowermost samples) due to an age inversion.

Age model for 5TC is based on the extrapolation of sedimentation rates estimated from ^{210}Pb data in the top 15 cm (McKay et al., 2008).

Supplement 4. IP$_{25}$ data for Canadian Archipalego straits (Vare et al., 2009; Belt et al., 2010).

ARC3 age (ka BP)	IP$_{25}$ (μg/cm^3)	ARC3 age (ka BP)	IP$_{25}$ (μg/cm^3)	ARC3 age (ka BP)	IP$_{25}$ (μg/cm^3)	ARC3 age (ka BP)	IP$_{25}$ (μg/cm^3)	ARC3 age (ka BP)
0.439	82.41306	0.754	44.53322	1.134	44.32754	1.525	71.27597	2.070
0.445	58.23777	0.761	42.38097	1.142	41.89352	1.534	74.67072	2.080
0.451	63.39468	0.768	45.08326	1.149	48.79968	1.543	80.22147	2.091
0.457	62.47043	0.774	47.09714	1.157	47.76535	1.551	69.54712	2.101
0.463	61.69971	0.781	34.29912	1.164	39.58121	1.560	64.16439	2.112
0.469	53.25025	0.788	33.36906	1.172	41.93291	1.568	65.11014	2.122
0.475	62.16344	0.794	35.37942	1.180	49.2897	1.577	76.6094	2.133
0.481	84.96272	0.801	43.60646	1.187	60.66468	1.586	61.78353	2.143
0.487	76.28586	0.808	54.58942	1.195	52.60376	1.595	75.31275	2.154
0.494	65.3379	0.815	48.44235	1.202	55.2028	1.603	64.47599	2.165
0.500	80.72261	0.821	45.40569	1.210	49.9238	1.612	74.73057	2.176
0.506	59.24046	0.828	48.10599	1.218	58.7962	1.621	75.85774	2.186
0.512	58.35774	0.835	41.03139	1.225	52.91357	1.630	67.73585	2.197
0.518	52.66865	0.842	51.41231	1.233	59.28315	1.639	82.30097	2.208
0.524	57.73207	0.849	48.06116	1.241	45.74345	1.648	72.27564	2.219
0.530	71.10681	0.855	47.86533	1.249	50.11044	1.656	83.64074	2.230
0.537	58.5296	0.862	52.24216	1.257	89.26092	1.665	75.39095	2.241
0.543	51.6196	0.869	46.06327	1.264	63.67588	1.674	70.77239	2.252
0.549	67.88439	0.876	47.75357	1.272	59.75923	1.683	64.46665	2.263
0.555	59.45424	0.883	50.74356	1.280	60.17878	1.692	72.80756	2.275
0.562	43.44536	0.890	54.4456	1.288	66.26534	1.701	82.96062	2.286
0.568	43.64842	0.897	50.32185	1.296	59.89478	1.711	81.24551	2.297
0.574	37.14538	0.904	61.91474	1.304	62.5327	1.720	76.55556	2.308
0.580	53.5387	0.911	63.15508	1.311	55.94704	1.729	65.71068	2.320
0.587	42.55508	0.918	55.44868	1.319	58.15393	1.738	66.51334	2.331
0.593	41.10164	0.925	58.53018	1.327	74.42158	1.747	49.50808	2.343
0.599	49.54989	0.932	49.67728	1.335	66.9409	1.756	50.66026	2.354
0.606	58.48141	0.939	46.17622	1.343	50.03299	1.766	52.87156	2.366
0.612	54.92025	0.946	55.45318	1.351	52.31297	1.851	64.18932	2.377
0.618	49.79066	0.995	28.22011	1.359	51.11277	1.860	77.29797	2.389
0.625	59.61241	1.002	35.08861	1.368	55.86571	1.870	68.89705	2.401
0.631	57.00945	1.010	30.85129	1.376	46.94738	1.880	62.39917	2.413
0.637	77.44746	1.017	29.25062	1.384	47.50101	1.889	82.92173	2.424
0.644	66.43769	1.024	31.24774	1.392	69.99137	1.899	78.20434	2.436
0.650	40.88245	1.031	30.96943	1.400	56.74799	1.909	70.57343	2.448
0.663	63.22517	1.039	29.74535	1.408	70.36187	1.928	79.16893	2.460
0.669	60.29464	1.046	37.62562	1.416	56.70904	1.938	81.58755	2.472
0.676	54.47634	1.053	74.6273	1.425	64.91482	1.948	70.45373	2.484
0.682	50.71657	1.060	63.9181	1.433	73.82989	1.958	78.66641	2.497
0.689	54.77308	1.068	56.88569	1.441	91.70935	1.968	81.40771	2.509
0.695	46.56717	1.075	72.38741	1.450	71.49726	1.978	88.90565	2.521
0.702	66.03172	1.082	46.58665	1.458	81.70865	1.988	84.90657	2.533
0.715	25.00364	1.090	49.34856	1.466	77.96529	1.998	79.26496	2.546
0.722	53.45188	1.097	32.98532	1.475	68.00339	2.008	74.24254	2.558
0.728	53.92145	1.105	39.52088	1.483	76.16941	2.019	81.20007	2.571
0.735	42.79376	1.112	47.64829	1.491	71.95818	2.029	75.52693	2.583
0.741	69.19097	1.119	37.6094	1.508	79.42157	2.049	90.8444	2.596
0.748	56.52325	1.127	39.49992	1.517	55.40689	2.060	83.73464	2.609

IP_{25} (μg/cm^3)	ARC3 age (ka BP)	IP_{25} (μg/cm^3)	ARC3 age (ka BP)	IP_{25} (μg/cm^3)	ARC3 age (ka BP)	IP_{25} (μg/cm^3)	ARC3 age (ka BP)	IP_{25} (μg/cm^3)
76.5026	2.622	83.89068	3.380	63.28418	4.419	45.06751	6.123	41.44527
77.39491	2.634	91.3248	3.398	57.24092	4.447	45.51426	6.165	41.614
72.32941	2.647	90.71851	3.416	52.58387	4.474	45.45806	6.208	42.13835
82.46023	2.660	97.2691	3.433	64.25813	4.502	42.94695	6.249	39.24287
80.38418	2.673	109.3075	3.451	65.63111	4.531	53.19953	6.291	39.52696
76.87324	2.686	92.80315	3.469	53.5832	4.559	44.90339	6.333	39.81564
74.28274	2.700	119.1311	3.488	54.25416	4.588	45.61246	6.375	35.59242
70.17589	2.713	84.34614	3.506	66.32499	4.617	45.04838	6.416	33.47574
115.963	2.726	92.84856	3.525	56.58374	4.647	39.25764	6.458	28.35548
95.97399	2.740	107.7825	3.543	59.41708	4.677	38.60414	6.499	22.00214
89.9455	2.753	104.0732	3.562	63.01974	4.707	41.83318	6.540	29.60853
87.72356	2.767	110.3097	3.581	62.09671	4.738	40.77591	6.581	29.98966
87.95473	2.780	111.8746	3.600	62.71083	4.769	39.80017	6.621	30.74899
91.20028	2.794	100.1264	3.619	69.49687	4.800	46.46244	6.661	26.81754
81.32451	2.808	72.16047	3.639	62.56641	4.832	44.6429	6.701	36.33435
81.23376	2.821	84.45689	3.658	57.26737	4.864	38.71932	6.741	40.70237
74.96168	2.849	76.71126	3.678	61.5923	4.897	43.25844	6.780	38.47879
94.13824	2.863	76.16178	3.698	73.09078	4.930	39.22214	6.819	40.02414
94.26425	2.878	78.12018	3.718	57.72916	4.963	34.11504	6.857	33.32826
91.02894	2.892	69.85483	3.739	54.6091	4.997	49.63603	6.896	29.59792
86.26409	2.906	69.7917	3.759	46.88097	5.031	41.33094	6.934	34.3129
83.39891	2.920	76.46058	3.780	54.47011	5.065	49.723	6.971	29.22927
78.94738	2.935	72.64896	3.801	46.21226	5.100	43.42815	7.008	33.1345
88.30618	2.950	69.48339	3.822	55.15391	5.135	45.83978	7.045	30.78417
91.47748	2.964	65.48372	3.843	67.06872	5.171	48.00954	7.081	31.79714
122.1987	2.979	64.66471	3.864	59.85476	5.207	39.74008	7.117	36.66097
101.2963	3.024	106.2943	3.886	58.94093	5.243	38.32268	7.153	28.40432
113.3267	3.039	88.99383	3.908	53.42199	5.280	40.99075	7.188	32.07201
134.3057	3.054	97.76734	3.930	50.86874	5.317	53.41946	7.223	39.45764
111.3344	3.069	85.73538	3.952	49.91138	5.355	38.45235	7.257	34.99634
133.0262	3.085	94.92214	3.974	45.63615	5.393	51.82148	7.291	29.61412
171.0329	3.100	69.57873	3.997	46.59388	5.431	48.32957	7.325	37.26502
129.1514	3.116	72.88858	4.020	49.468	5.470	47.87932	7.358	36.56044
71.67323	3.132	73.23066	4.043	44.90301	5.509	43.20417	7.391	35.87196
75.12555	3.147	73.87261	4.066	45.92766	5.548	47.32126	7.423	34.53413
88.3094	3.163	65.89188	4.090	53.53935	5.587	44.20571	7.455	34.34586
96.81662	3.179	79.8956	4.114	44.63755	5.627	39.15393	7.487	33.24527
84.79498	3.195	64.89104	4.138	40.07699	5.668	43.60826	7.518	37.13224
74.56976	3.212	56.67447	4.162	52.07288	5.708	42.41195	7.549	29.4772
78.46497	3.228	69.13965	4.186	47.54885	5.749	46.52673	7.580	36.65962
70.35996	3.244	54.31424	4.211	47.01472	5.790	42.35367	7.610	36.19456
68.26434	3.261	61.13478	4.236	46.33566	5.831	45.25676	7.640	35.76249
52.88752	3.278	62.77476	4.262	47.03839	5.872	40.04896	7.670	33.67537
73.37863	3.295	59.86044	4.287	38.39895	5.914	41.27688	7.699	35.3278
70.07608	3.311	61.18854	4.313	44.36341	5.956	38.19957	7.728	41.16366
93.8549	3.328	60.28895	4.339	43.0057	5.998	34.85425	7.756	40.38431
79.19348	3.346	60.41681	4.366	35.52165	6.039	38.61751	7.785	25.14805
98.12664	3.363	72.43975	4.392	47.97308	6.081	35.07647	7.813	35.84466

ARC3 age (ka BP)	IP_{25} (µg/cm^3)	ARC3 age (ka BP)	IP_{25} (µg/cm^3)	ARC3 age (ka BP)	IP_{25} (µg/cm^3)
7.840	30.34464	8.974	21.76476	9.689	18.04971
7.867	27.30513	8.991	19.3742	9.702	14.49269
7.894	31.82337	9.008	14.57122	9.714	15.83969
7.921	31.532	9.024	17.03517	9.727	13.71912
7.948	30.67311	9.041	15.90193	9.739	14.98147
7.974	22.39194	9.057	20.66135	9.751	14.42737
8.000	26.57523	9.074	21.35222	9.764	11.40259
8.025	26.23701	9.090	18.9632	9.776	19.99068
8.050	26.15725	9.106	15.44031	9.788	13.19881
8.075	22.32561	9.122	17.17393	9.800	14.97622
8.100	22.61204	9.138	17.63149	9.813	16.69845
8.125	21.39967	9.154	15.89273	9.825	14.93752
8.149	16.2402	9.169	17.01131	9.837	17.55207
8.173	16.21681	9.185	15.38527	9.849	14.38155
8.197	16.6812	9.201	19.02599	9.860	10.256
8.220	17.28195	9.216	19.04808	9.872	19.12112
8.244	19.29266	9.231	17.42531	9.884	10.90892
8.267	16.09532	9.246	20.47077	9.896	15.54094
8.289	20.53391	9.262	20.93101	9.907	14.41808
8.312	18.45421	9.277	16.78431	9.919	12.41311
8.334	15.22158	9.291	18.04688	9.931	10.4353
8.357	20.40512	9.306	13.30203	9.942	14.11761
8.379	20.74537	9.321	19.74675	9.952	10.11394
8.400	17.23083	9.350	16.40506	9.965	8.981253
8.422	17.56554	9.365	15.31968	9.976	10.41085
8.443	15.55052	9.379	15.52711	9.988	11.39778
8.465	17.14784	9.393	13.71019	9.999	13.37487
8.486	20.63835	9.408	20.08986	10.010	15.25147
8.506	20.52492	9.422	16.38811	10.021	11.71146
8.527	19.57209	9.436	16.45074		
8.547	16.65188	9.450	16.29395		
8.568	16.0779	9.464	19.46252		
8.588	17.72991	9.478	17.84784		
8.608	15.51211	9.491	18.2295		
8.627	17.59603	9.505	16.80523		
8.647	20.99199	9.519	15.95937		
8.761	15.06834	9.532	17.80457		
8.780	15.24279	9.546	16.11275		
8.798	17.92198	9.559	20.3416		
8.816	16.85476	9.572	15.38938		
8.834	16.19101	9.585	19.57632		
8.852	16.06783	9.599	18.93073		
8.870	15.27088	9.612	22.19426		
8.888	16.02739	9.625	16.98569		
8.905	18.64322	9.638	21.28948		
8.923	15.5264	9.651	19.05812		
8.940	14.72557	9.663	15.96682		
8.957	22.7931	9.676	15.47729		

ARC4 age (ka BP)	IP_{25} (µg/cm^3)	ARC4 age (ka BP)	IP_{25} (µg/cm^3)	ARC4 age (ka BP)	IP_{25} (µg/cm^3)	ARC4 age (ka BP)	IP_{25} (µg/cm^3)
0.083	12.32416	2.092	1.89332	3.498	2.516762	7.062	0.737928
0.120	12.88982	2.100	3.52285	3.656	3.859104	7.129	0.463309
0.193	16.73381	2.116	3.018899	3.705	3.127487	7.196	2.699002
0.229	11.47175	2.148	2.060493	3.756	4.119796	7.285	2.377605
0.299	19.60769	2.171	1.881046	3.824	3.886195	7.419	0.844654
0.367	6.29435	2.193	2.795593	3.877	3.502511	7.508	1.10349
0.433	8.395601	2.221	1.974745	3.931	2.186379	7.642	1.410636
0.529	5.997806	2.242	2.011742	4.004	2.550917	7.731	0.176598
0.560	4.609663	2.262	2.703038	4.060	2.309685		
0.621	10.48731	2.289	2.06045	4.116	2.745695		
0.681	2.822772	2.308	1.891092	4.193	2.954294		
0.738	3.97289	2.327	2.6038	4.252	1.960109		
0.822	6.083625	2.353	2.559701	4.312	1.847037		
0.849	3.544594	2.372	1.694873	4.392	3.225166		
0.902	5.133873	2.391	1.81657	4.454	3.002472		
0.953	2.470245	2.416	2.60765	4.516	2.091939		
1.003	2.645923	2.435	1.85443	4.600	2.194223		
1.075	2.538784	2.455	1.485349	4.663	2.349346		
1.099	2.050255	2.481	3.138348	4.728	2.375441		
1.144	3.493423	2.500	2.03431	4.880	2.63388		
1.189	2.471122	2.520	2.378105	4.946	2.030091		
1.232	2.239983	2.548	2.905159	5.035	2.941175		
1.294	2.203757	2.569	1.783695	5.102	3.196853		
1.314	2.198746	2.590	2.447233	5.170	1.988816		
1.354	3.49186	2.619	2.135826	5.260	2.162027		
1.392	2.966023	2.642	1.40055	5.328	3.514437		
1.429	3.171271	2.665	1.75598	5.397	1.67142		
1.482	3.640119	2.697	2.94557	5.488	2.3457		
1.598	4.71347	2.722	1.639954	5.557	3.050309		
1.613	3.669	2.747	2.072719	5.625	3.304475		
1.687	4.261391	2.782	2.129257	5.717	4.791918		
1.715	2.248968	2.810	1.387098	5.785	3.724849		
1.743	2.530841	2.838	1.909039	5.854	4.705797		
1.782	2.397184	2.876	2.289102	5.945	3.599533		
1.795	3.659106	2.906	1.898797	6.012	2.493909		
1.819	3.083397	2.937	2.027467	6.080	1.938833		
1.843	2.382163	2.979	2.159918	6.169	2.32285		
1.867	2.160701	3.012	1.665293	6.236	1.873356		
1.900	2.262214	3.046	2.290975	6.303	1.813004		
1.911	5.57003	3.093	1.574686	6.392	3.463919		
1.933	3.510386	3.129	2.029939	6.459	1.264171		
1.953	4.065737	3.166	2.504244	6.526	0.979116		
1.974	2.898033	3.217	2.581907	6.615	2.46075		
2.003	1.799525	3.256	2.159031	6.682	1.421373		
2.012	2.674056	3.296	2.498021	6.749	1.273596		
2.031	2.819281	3.352	2.103438	6.838	0.774586		
2.049	4.212454	3.394	2.602553	6.905	0.484143		
2.066	1.782172	3.438	3.049314	6.972	0.462931		

ARC5 age (ka BP)	IP_{25} (µg/cm^3)	ARC5 age (ka BP)	IP_{25} (µg/cm^3)
0.584	3.6128	3.603	1.911786
0.746	1.796658	3.689	1.504746
0.847	1.579363	3.826	1.73249
0.991	0.874117	3.923	1.487132
1.081	1.502326	4.077	1.629485
1.207	1.035866	4.186	1.272275
1.287	1.498005	4.360	1.436248
1.398	0.953612	4.483	1.618653
1.467	1.385976	4.677	1.912881
1.625	1.613986	4.814	1.539255
1.710	1.04214	5.030	1.479247
1.762	1.489122	5.182	1.67492
1.836	1.604007	5.422	2.029708
1.882	2.364801	5.591	2.221957
1.945	1.659016	5.856	2.767407
1.985	1.312277	6.041	1.497384
2.041	1.122432	6.332	1.854354
2.076	1.462214	6.536	1.736745
2.125	1.546667	6.855	1.518671
2.155	1.462387	7.077	1.665361
2.199	1.254345	7.426	1.977946
2.227	1.090435	7.668	1.501966
2.266	1.212083	8.048	2.120754
2.292	1.028057	8.311	1.88046
2.329	0.849536	8.723	2.047955
2.354	1.264128	9.008	1.404723
2.390	1.736147	9.453	2.412902
2.414	1.518516	9.761	1.747788
2.451	1.67466	10.242	2.057612
2.476	1.403361	10.574	1.823924
2.514	1.748827	11.090	1.857204
2.541	1.498773	11.447	1.810214
2.583	2.208207		
2.612	1.540533		
2.659	1.69515		
2.692	1.769992		
2.745	1.570727		
2.783	1.400565		
2.843	1.602438		
2.887	1.279171		
2.956	2.149344		
3.006	1.80913		
3.086	2.053442		
3.144	1.522046		
3.236	1.757501		
3.302	1.356784		
3.407	2.185057		
3.483	1.87372		